ORIGINAL PAPER

Pre-eruptive conditions and triggering mechanism of the ~ 16 ka Santa Bárbara explosive eruption of Sete Cidades Volcano (São Miguel, Azores)

Kathrin Laeger[1] · Maurizio Petrelli[1] · Daniele Morgavi[1] · Michele Lustrino[2,3] · Adriano Pimentel[4,5] · Joali Paredes-Mariño[1] · Rebecca L. Astbury[1] · Ulrich Kueppers[6] · Massimiliano Porreca[1] · Diego Perugini[1]

Abstract

The Santa Bárbara trachytic eruption (~ 16 ka) was one of the major eruptions of the Sete Cidades Volcano (São Miguel Island, Azores), recording the last phase of caldera formation. Here, we report and combine geochemical, mineralogical, and petrological constraints on natural samples with time-series experiments to describe the pre-eruptive conditions of the Santa Bárbara plumbing system. The trachytic pumice clasts are notably characterized by the presence of hawaiitic enclaves, banded textures (~ 60–67 wt% SiO_2) and high variability in mineral phases, occasionally rounded and partially resorbed. The hawaiitic enclaves contain quench textures such as sharp contacts with the trachytic groundmass, as well as acicular and skeletal growth of several minerals, pointing to a high-temperature gradient between the hot hawaiitic magma and the colder trachytic reservoir. Distinct phenocryst rim compositions in both magmas exclude significant chemical diffusion. We suggest that the hawaiitic enclaves represent an intrusion that triggered the eruption, but was only partially involved in the mixing process that generated the banded groundmass textures. These textural heterogeneities are interpreted to be related to a self-mixing event induced by convection within a compositionally zoned reservoir, with trachytic and mugearitic magmas at the top and the bottom, respectively. In detail, the model requires the likely arrival of hawaiitic magma to the base of the reservoir, inducing mixing by reheating of the resident mugearitic magma and volatile transfer. These processes produced a thermo-chemical destabilization (i.e., convection) of the shallow reservoir and mixing between the mugearitic and the trachytic magmas. We reproduced the observed chemical signatures performing time-series mixing experiments and calculated the concentration variance decay during mixing. Estimated timescales indicate that the hawaiitic intrusion took place ~ 41 h before the onset of the eruption.

Keywords Azores · Fractional crystallization · Homogenization · Mafic enclaves · Magma mixing · Time-series experiments

Introduction

Sete Cidades Volcano (SCV) is one of three active trachytic central volcanoes on the island of São Miguel (Azores), and the volcano with the highest eruptive frequency in the Azores over the last 5 ka (Cole et al. 2008; Queiroz et al. 2008, 2015). Earlier studies focused on the geological setting, the stratigraphy of SCV (Booth et al. 1978; Moore 1990, 1991a, 1991b; Queiroz 1997; Queiroz et al. 2008, 2015) and the evolution of the volcanic plumbing system (Mattioli et al. 1997; Renzulli and Santi 2000; Beier et al. 2006).

The activity of SCV can be divided into three stages: (1) a shield-building stage, corresponding to the subaerial

construction of the volcanic edifice (basaltic and trachytic magmatism); (2) a caldera-forming stage, dominated by at least three paroxysmal events (trachytic magmatism); and (3) a post-caldera stage, characterized by intra-caldera explosive volcanism and flank eruptions (mostly trachytic and subordinate basaltic magmatism) (Queiroz 1997; Beier et al. 2006; Queiroz et al. 2015).

The petrological evolution of SCV magmas during the subaerial eruptive period (< 210 ka) is mainly described as a result of two-step fractional crystallization, where mafic melts rise from the mantle, stagnate, and fractionate close to the Moho (~ 15 km depth), followed by later accumulation of evolved melts in the shallow crust (~ 3 km depth; Renzulli and Santi 2000; Beier et al. 2006). Overall, rock compositions and petrologic relations between minerals and glasses show that SCV products follow a single liquid line of descent (Mattioli et al. 1997; Renzulli and Santi 2000; Beier et al. 2006). The transition from hawaiite to trachyte can be achieved through the crystallization of plagioclase, clinopyroxene, kaersutite, and magnetite (Mattioli et al. 1997; Renzulli and Santi 2000; Beier et al. 2006). Magma mixing/mingling between mafic and felsic magmas also seems to play a significant role at SCV (Beier et al. 2006). In particular, the intrusion of basaltic magma into a shallow trachytic reservoir has been proposed as the triggering mechanism of paroxysmal explosive eruptions associated with caldera formation (Beier et al. 2006; Queiroz et al. 2015; Porreca et al. 2018). Yet, a detailed petrological study about the magmamixing/mingling processes related to caldera-forming eruptions at SCV is still missing.

This study aims to provide new insights on the magmatic evolution of the SCV plumbing system, through a detailed investigation of the pyroclastic rocks from the Santa Bárbara (SB) Formation, focusing on the magma-mixing processes and supporting the findings on natural samples with experimental data. The SB Formation records one of the major explosive eruptions that occurred in São Miguel Island (~ 16 ka) and corresponds to the last phase of caldera enlargement of the SCV (Queiroz 1997; Queiroz et al. 2015; Porreca et al. 2018). The products of the SB Formation are characterized by the presence of mafic enclaves (~ 49 wt% SiO_2, ~ 4.9 wt% MgO) dispersed within pumice clasts (~ 62–66 wt% SiO_2, ~ 0.2 wt% MgO), attesting to the intrusion of hawaiitic magma in a trachytic magma reservoir (Queiroz 1997; Queiroz et al. 2015; Porreca et al. 2018). Such an intrusion would imply cooling and possibly quenching, followed by disruption of hawaiitic magma when in contact with the colder trachytic magma. This would subsequently cause boosted bubble nucleation and growth, leading to accelerated and enhanced eruption explosivity (Paredes-Mariño et al. 2017). Nevertheless, pressure and temperature estimates, as well as the water content of the plumbing system of the SB explosive eruption, are still poorly constrained and require further investigation. Here, we present new mineral and whole-rock geochemical data, as well as petrological constraints on glasses and minerals. Mixing experiments reproduced the compositional patterns in the groundmass glasses to quantify timescales of homogenization. Finally, we combine the results from geochemical modeling and experiments to draw a complete picture of the pre-eruptive magma dynamics, which explains the compositional and petrological features observed in SB eruptive products.

Geological background

São Miguel is the largest island of the Azores archipelago, situated ~ 350 km east of the Mid-Atlantic Ridge, along the axis of the Terceira Rift (TR) that divides the Eurasian plate from the Nubian plate (Fig. 1a, e.g., Machado 1959; Kraus and Watkins 1970; Schilling 1975; Luis et al. 1994; Widom and Shirey 1996; Gente et al. 2003; Beier et al. 2006; Miranda et al. 2015). Subaerial volcanism of São Miguel dates back to more than 0.8 Ma (Johnson et al. 1998; Sibrant et al. 2015). Active volcanism is concentrated on three trachytic central volcanoes, Sete Cidades (SCV), Fogo (also known as Água de Pau) and Furnas, separated by basaltic fissure systems (Picos and Congro fissure systems; Fig. 1b; Gaspar et al. 2015).

The SCV edifice is located in the western part of São Miguel Island and is strongly controlled by the NW–SE striking TR axis (Fig. 1a, b). Currently, SCV reaches a maximum altitude of 845 m asl and occupies a surface area of ~ 110 km², with a subaerial diameter of ~ 12 km (Queiroz et al. 2008, 2015). It is characterized by a sub-circular summit caldera ~ 5 km in diameter (~ 350 m deep, on average). The caldera is largely occupied by lakes and filled by pumice cones, maars, tuff rings/cones, and remnants of lava domes (Fig. 1c; Queiroz et al. 2008, 2015; Porreca et al. 2018).

Stratigraphy and eruptive history of Sete Cidades Volcano

According to the scheme of Queiroz (1997) and Queiroz et al. (2015), the stratigraphy of SCV is organized into two groups. The Inferior Group is formed by all the volcanic products older than ~ 36 ka. The oldest rock of SCV is dated to ~ 210 ka (Moore 1990). This group includes basaltic-to-trachytic lavas and minor pyroclastic deposits. The Superior Group is composed of products younger than ~ 36 ka. It comprises, alongside other deposits, the major trachytic pyroclastic formations associated with three phases of caldera formation, dated ~ 36, ~29, and ~ 16 ka (Queiroz 1997). At least 17 intra-caldera trachytic pumice deposits and more than 12 flank basaltic lavas and scoriae are recognized in the
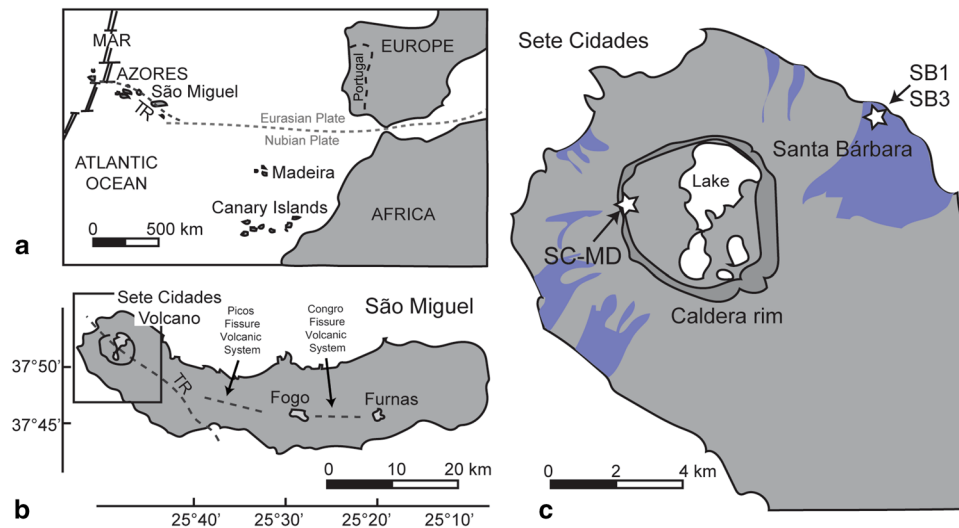
Fig. 1 **a** Map of the North Atlantic Ocean with the location of Azores archipelago east from the Mid-Atlantic Ridge (MAR) along the Terceira Rift (TR) axis. **b** Map of São Miguel Island illustrating the active volcanic systems, the position of the Terceira Rift axis and the Congro Fissure System (CFS) and associated tectonic features. **c** Sete Cidades Volcano with mapped deposits of the Santa Bárbara Formation (light blue areas). Samples SB1 and SB3 were taken from a location near Santa Bárbara parish. Sample SC-MD was collected from a dyke situated in the inner western caldera wall of Sete Cidades

last 5 ka (Booth et al. 1978; Queiroz 1997; Queiroz et al. 2008, 2015).

The shield-building stage lasted from > 210 to ~ 36 ka was dominated by effusive volcanism and corresponds to the subaerial growth of the central volcanic edifice. This was followed by the caldera-forming stage between ~ 36 and ~ 16 ka, marked by at least three paroxysmal explosive eruptions associated with different phases of the caldera formation. The post-caldera stage ranges from ~ 16 ka to present-day, characterized by numerous intra-caldera sub-Plinian eruptions, frequently hydromagmatic, and coeval low-explosivity/effusive flank eruptions (Queiroz 1997; Beier et al. 2006; Queiroz et al. 2015). Chemical compositions of the SCV products define a classical mildly alkaline sodic series, ranging from alkali basalt, over hawaiite to trachyte, with rare mugearite and even rarer benmoreite (Fig. 2; Moore 1990, 1991b; Renzulli and Santi 2000; Beier et al. 2006; Queiroz et al. 2015). Evidence of magma mixing is often reported in the volcanic products of the SCV, although its effect is still not evaluated in detail.

The plumbing system of Sete Cidades Volcano

Renzulli and Santi (2000) quantified the presence of two storage levels beneath SCV at 400 MPa (~ 13 km depth) and 1220 ± 60 °C (based on ternary feldspars and olivine–melt equilibria) for primitive magmas and 20–150 MPa (~ 0.5-5 km depth) and at least ~ 700 °C for more evolved ones. Similarly, Beier et al. (2006) estimated P–T conditions, via pyroxene–liquid equilibria, of 550 ± 170 MPa (~ 16.5 km depth) and 1175 ± 30 °C for mildly evolved magma (5.5–6.5 wt% MgO) and 420 ± 170 MPa (~ 14.8 km depth) and ~ 1035 °C for evolved products (~ 2.4 wt% MgO). In addition, Beier et al. (2006) reported P–T conditions for two stagnation levels at shallower crustal depths corresponding to 110 ± 30 MPa (~ 3.5 km depth) and 820 °C for highly evolved melts, and at 300 ± 70 MPa (~ 10.6 km depth) for mafic to intermediate melts. Despite these estimates, P and T constraints of single eruptive events during the caldera-forming stage are still missing.

Gravity models indicate a crustal thickness of 10–15 km for the Azores Plateau east of the Mid-Atlantic Ridge (Wang et al. 2011). Close to the Moho, primary magmas stagnate and fractionate to hawaiitic compositions which rise further into the crust (Renzulli and Santi 2000). At a shallow depth of ~ 0.5–5 km (20–150 MPa, inferred by the geobarometer of Green and Usdansky 1986), intermediate magmas stagnate and differentiate to form evolved reservoirs (Renzulli and Santi 2000; Beier et al. 2006).

Conversely, in the post-caldera stage, a deeper magma storage level was probably located at a depth of ~ 15–16 km, close to the Moho (Luis et al. 1998; Escartín et al. 2001). The described multi-step model of an initial deeper storage level in the upper mantle–crust boundary, followed by ascent and accumulation at shallower depth is commonly envisaged to occur beneath other volcanoes of the Azores, such as Caldeira Volcano (Faial; Zanon and Frezzotti 2013; Pimentel et al. 2015), Pico Alto Volcano (Terceira; Zanon and Pimentel 2015; Jeffery et al. 2017), Furnas Volcano (São Miguel; Jeffery et al. 2016) and Atlantic oceanic islands (e.g., Klügel
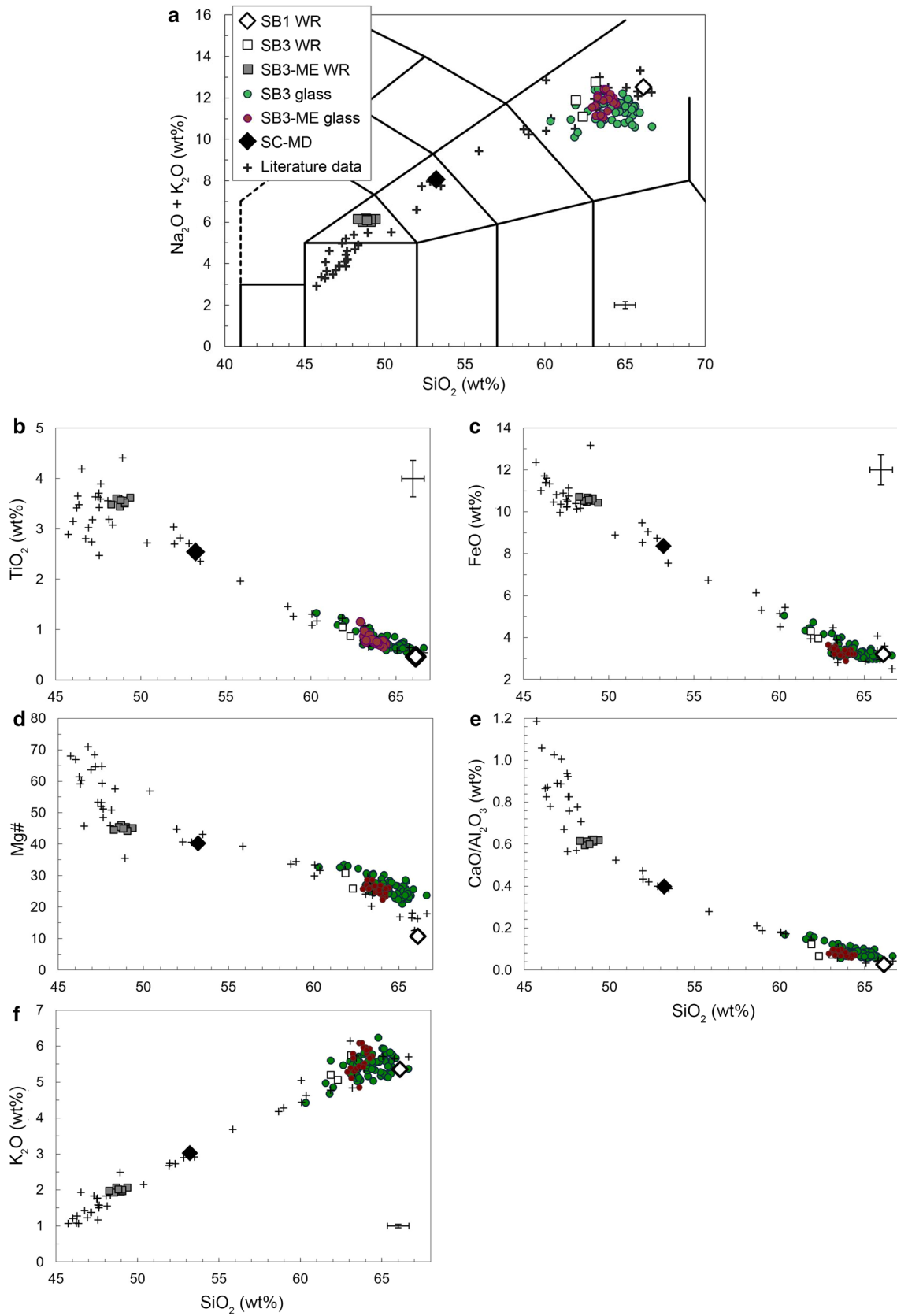
◄**Fig. 2 a** Total alkali versus silica diagram after Le Maitre et al. (2002), and **b–f** selected major element versus silica diagrams showing whole-rock (WR) compositions (normalized to 100%) of Santa Bárbara products (squares), of the mafic and felsic end-members used for time-series experiments (diamonds) and glass compositions of SB3 products (circles). Note that all compositions presented in this study correlate well with the trend of rock compositions, available in the literature (crosses), from the entire history of Sete Cidades (Renzulli and Santi 2000; Beier et al. 2006; Queiroz et al. 2015). SB1—white pumices, SB3—banded pumices, SB3-ME—mafic enclaves, SC-MD—mugearitic dyke

et al. 2000, 2005; Renzulli and Santi 2000; Schwarz et al. 2004; Beier et al. 2006).

The Santa Bárbara formation

The Santa Bárbara (SB) Formation records the last major explosive event of the caldera-forming stage of SCV and is dated at $15{,}740 \pm 200$ years (uncalibrated ^{14}C years BP; Queiroz 1997). It is composed of a pyroclastic succession divided into Lower, Middle and Upper Members (Queiroz 1997; Queiroz et al. 2015; Porreca et al. 2018). The Lower Member consists of a sequence of alternating ash and fine-grained pumice lapilli beds, interpreted as ash/pumice fall and dilute pyroclastic density current deposits. The Middle Member is composed of coarse-grained pumice and lithic-rich ignimbrites, deposited from high particle concentration pyroclastic density currents. The Upper Member corresponds to coarse-grained pumice lapilli fall deposits, with asymmetric distribution pattern that probably affected the entire north coast of São Miguel Island (Kueppers et al. 2019). A detailed description of the stratigraphic succession is reported in Porreca et al. (2018). One of the characteristic features of the SB Formation is the presence of white and banded trachytic pumice clasts containing dark hawaiitic enclaves, with increasing abundance upward through the pyroclastic succession (Porreca et al. 2018). The heterogeneities found in the SB formation may reflect the presence of various magma batches that mixed before the eruption. The typical mineral assemblage of the hawaiitic enclaves consists of olivine, clinopyroxene, feldspars, amphibole, and apatite (Queiroz 1997).

Methods

Selection and preparation of natural samples

Samples were collected from the Lower and Upper Members (SB1 and SB3, respectively) of the SB Formation, on the NE flank of SCV (Fig. 1c). Sample SC-MD corresponds to a mugearite dyke, located in the inner west caldera wall of SCV. Sampled volcanic products consist of white pumice clasts (sample SB1), banded pumice clasts (SB3) and mafic enclaves (SB3-ME). Polished thin sections of pumice clasts of sample SB3 were prepared for petrographic observation and chemical analyses of glasses and minerals.

Chemical analyses

Major element analyses of minerals and glasses

Major element concentrations of minerals and glasses were determined for natural and experimental samples via electron microprobe (EMP) CAMECA SX50 at the CNR Istituto di Geologia Ambientale e Geoingegneria in the Dipartimento di Scienze della Terra in Rome (Italy). The EMP is equipped with four wavelength-dispersive spectrometers and 12 crystals. The electron beam had a current of 15 nA, an accelerating voltage of 15 keV. A focused and defocused beam diameter of 10 μm was used for minerals and glasses, respectively, utilizing 20 s counting times for each element. Synthetic and natural standards were used for calibration. In detail: wollastonite (Si and Ca), corundum (Al), diopside and olivine (Mg), magnetite (Fe), rutile (Ti), orthoclase (K), jadeite (Na), phlogopite (F), KCl (Cl), barytine (S), apatite (P), and standard metals (Mn, Ni, and Cr). Three international secondary standards (Kakanui augite, Icelandic Bir-1 and rhyolite RLS132 glasses from USGS) were measured prior to any series of measurements. Sodium and potassium were analyzed first to reduce possible volatilization effects. Errors on the accuracy were $< 2\%$ for SiO_2, TiO_2, Al_2O_3, TiO_2, FeO, MgO, and CaO and $< 5\%$ for Na_2O, K_2O, MnO, and P_2O_5. ZAF correction routines (Armstrong and Buseck 1975) were used to obtain element concentrations. Analysis of whole-rock compositions took place on randomly chosen spots on polished mounts of homogenized melts of SB1, SB3-ME, and SC-MD. The precision on the resulting homogenized glasses portions was always better than 10% ($n = 10$). Experiments were measured along transects through the filaments with an inter-point distance ranging from 20 to 300 μm. All chemical analyses are provided in the Electronic Supplementary Material (ESM).

Magma-mixing experiments

Selection of end-member compositions

The felsic end-member was prepared from sample SB1, consisting of white trachytic pumices (~ 66.0 wt% SiO_2, ~ 12.5 $Na_2O + K_2O$, ESM 1; Fig. 2), and representing the most evolved rocks of the SB Formation. The mafic end-member was prepared from sample SC-MD, of mugearitic composition (~ 53 wt% SiO_2, ~ 8.1 $Na_2O + K_2O$, ESM 1; Fig. 2).

Experimental setup

Rock samples were powdered, melted, and homogenized in a $Pt_{80}Rh_{20}$ crucible (~75 cm^3) at 1600 °C for 4 h followed by fast quenching in the air to ensure a homogeneous glass composition (water- and crystal-free). Two holes were drilled into the felsic end-member (SB1) to insert the mafic end-member (SC-MD) and an inner off-centered spindle (Fig. 3). Experiments were performed at 1200 °C with the ChaOtic Magma-Mixing Apparatus (COMMA) at the Department of Physics and Geology, University of Perugia (Morgavi et al. 2015).

The geometry of the system is characterized by two parameters: (a) the ratio of the radii of the two cylinders $r = R_{in}/R_{out} = 1/3$ and (b) the eccentricity ratio of the outer cylinder $\varepsilon = \delta/R_{out} = 0.3$, where δ is the distance between the centers of the two cylinders (Swanson and Ottino 1990). The mixing of magmas is triggered by the alternating rotations of the inner and the outer cylinder in opposite directions, because both streamlines and velocity are time-dependent (Swanson and Ottino 1990; Galaktionov et al. 2002). For the present work, the characteristic velocity $V = |V_{in}| + |V_{out}|$ and characteristic length $L = R_{out} - R_{in}$ are equal to 2.8×10^{-5} m s^{-1} and 1.23×10^{-2} m, respectively, with a strain rate of $\sim 10^{-3}$ s^{-1}, calculated in agreement with Galaktionov et al. (2002). In the reported fluid-dynamical conditions, the experimental Reynolds (*Re*) and Schmidt (*Sc*) numbers are 6.3×10^{-9} and 5.4×10^{14}, respectively.

In detail, the crucible and the spindle rotated alternatingly using the following mixing protocol: one full cycle consisted of two rotations of the crucible (210 min each) followed by six rotations, 36 min each, of the spindle, corresponding to ~10.5 h. Experiment 1 (EXP1) followed the protocol for one full cycle (~10.5 h), experiment 2 (EXP2) for two cycles (~21 h) and experiment 3 (EXP3) for four cycles (~42 h; Fig. 4). The temperature of 1200 °C was selected to proxy, using anhydrous melts, the rheological

(i.e., viscosities) and chemical (i.e., diffusivities) behavior of the hydrous magmas (with H_2O ranging between 2 and 4 wt%) at ~1000–1100 °C in agreement to a viscosity parameterization based on Giordano et al. (2008) and the diffusivity enhancement due to the addition of water reported by González-García et al. (2017). In detail, the logarithm of the viscosities at 1200 °C in dry conditions is ~2.9 and 4.2 for the mugearitic and trachytic end-members, respectively. These values are in good agreement with the logarithm of the viscosities for the same magmas at 1000 °C and 2 wt% of water that are ~2.8 and ~3.7, respectively. The viscosity ratio (λ) between the mugearitic and the trachytic end-members is ~0.1 and ~0.05 at 1000 °C, 2 wt% water and 1200 °C, dry conditions, respectively. In both the cases, $\lambda > 1$ in the same order of magnitude. Under these conditions, the expected evolution of the mixing process is similar and characterized by a rapid stretching, resulting in a quick homogenization (Manga 1996).

For the chemical diffusivities, the presence of ~2 wt% of water leads to an increase in the chemical diffusivities of ~1.5 log units compared to that of dry conditions (González-García et al. 2017). Assuming an Arrhenian behavior for the selected chemical species (e.g., Zhang et al. 2010), an increase in the temperature of ~200 °C agrees well with an increase in the chemical diffusivities of ~1.5 log units.

After successful runs of the protocols, the samples were quenched in air corresponding to a cooling rate of 50°C/min that prevent from quench crystallization. Subsequently, the samples (33 mm in diameter) were cored out, embedded in epoxy, cut into 4 mm slices, and polished for microanalysis. Sample mounts of homogenized melt of the two end-members (SB1 and SC-MD) and of the mafic enclaves (SB3-ME) were also prepared for comparison. It has been widely demonstrated that this experimental approach allows to follow in time and space the evolution of the mixing process between different magmas and the associated modulation of chemical composition (Morgavi et al. 2015). Also, Morgavi

Fig. 3 a Geometric relations of the mixing experiment after Morgavi et al. (2015). The ratio of Melt SB1 and Melt SC-MD is 88:12, respectively. *R_{out}* radius of outer cylinder = 18.5 mm, *R_{in}* radius of inner cylinder = 6.2 mm, *R_m* radius of the mafic end-member = 6.0 mm, and *δ* distance between the centers of inner and outer cylinder = 11.1 mm. **b** Photograph of $Pt_{80}Rh_{20}$ crucible with end-members and spindle inserted before EXP1
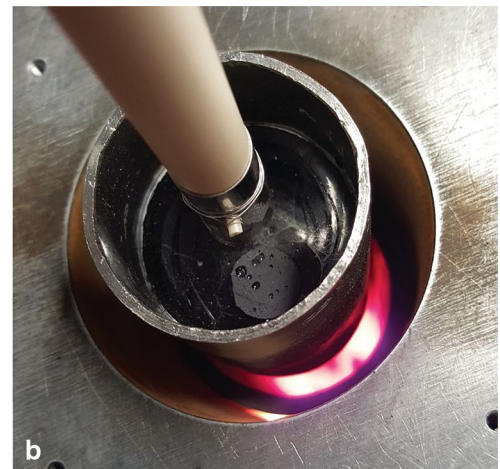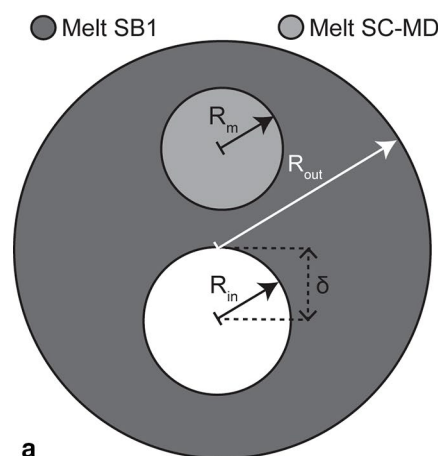
Fig. 4 BSE images of magma-mixing experiments EXP1, EXP2, and EXP3 that lasted ~ 10.5, 21, and 42 h, respectively, showing the filament-like structures composed by varying compositions between mugearite and trachyte. Note that filaments become finer and evolve a lower gradient (i.e., contrast) illustrating a higher degree of mixing with increasing run time of the experiments. Point distances are for transects EXP1-5_a-y—200 μm; EXP1-1_1-100—20 μm, EXP1-2_A-U—313 μm, EXP1-2_V-t—115 μm; EXP2-1A_1–10—10 μm, and EXP2-1B-D and EXP3-2A-C with 20 μm each
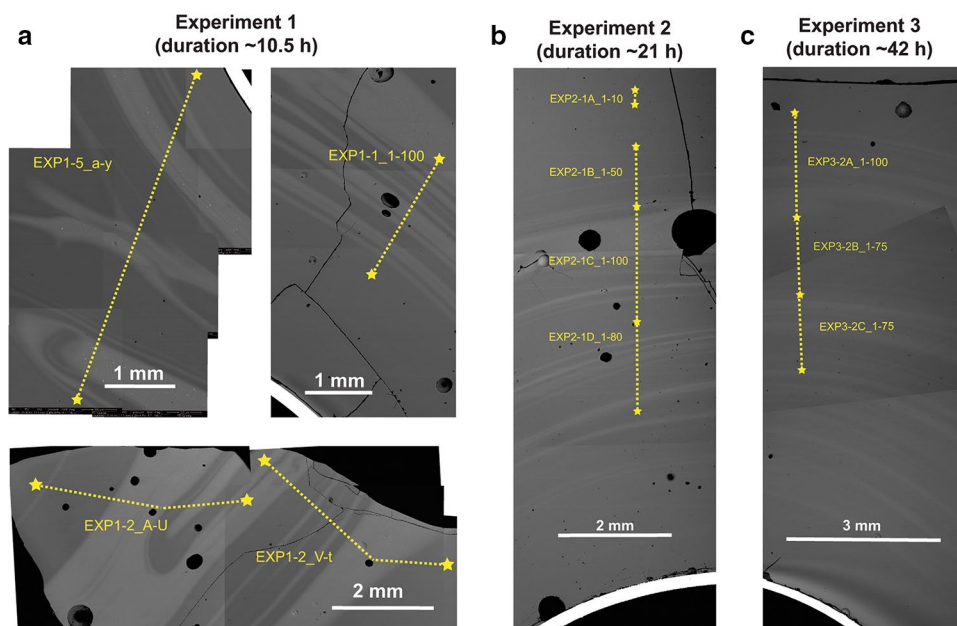
et al. (2015) showed that the generated mixing structures are topologically identical to those observed in natural volcanic rocks. As a drawback, the proposed experimental approach does not account for the influence of bubble and crystal development on the rheological evolution of the system. This is due to the fact that performing this kind of experiments under controlled pressure conditions is presently not feasible because of technical issues.

Scaling of the experiments to natural scenarios

As reported by Rossi et al. (2017), the proposed experimental approach can also be used to infer the timescales required to homogenize the compositional heterogeneity in natural magmatic systems using dimensional analysis.

The efficiency of mixing is a strong function of the Rayleigh (e.g., Petrelli et al. 2016, 2018) and Reynolds numbers (e.g., Huber et al. 2009). However, in cases, where chaotic dynamics occurs, mixing can also be efficient even at small Re numbers if enough time is allowed for the stirring to occur (Huber et al. 2009).

In general, to achieve homogenization, an efficient action of chemical diffusion is a required condition. In the absence of advection, the homogenization time only depends on the dimension of the system and chemical diffusivities. In particular, a blob characterized by a dimension L and a chemical diffusion coefficient D will homogenize in a time t_h proportional to L^2/D. We refer to t_h as the homogenization time of the chemical heterogeneity.

In the presence of advection, t_h can be expressed as a function of the Reynolds (Re) and Schmidt (Sc) numbers (Raynal and Gence 1997):

$$t_h \sim \frac{L^2}{\nu}\frac{1}{Re}f(ReSc), \qquad (1)$$

where ν is the kinematic viscosity, $Re = VL/\nu$ and $Sc = \nu/D$.

In chaotic systems characterized by $ReSc \gg 1$, as in the case of most of natural magmatic systems in dynamic conditions, t_h can be expressed as follows (Raynal and Gence 1997):

$$t_h \sim \frac{L^2}{\nu}\frac{1}{Re}\ln(ReSc). \qquad (2)$$

Equation 2 can be used to combine the results obtained experimentally with the dimension L of the system and the strength of advective flows (through Re), i.e., the vigour of stretching and folding dynamics. In particular, considering filaments of different thicknesses of one magma dispersing into a host magma, it is possible to estimate the time required to attain homogenization as a function of the Re, as mixing dynamics (i.e., the advective flows) develop in time (further details in Rossi et al. 2017).

Results

The petrographic descriptions of the studied natural samples (SB1, SB3, and SB3-ME) are reported in Tables 1 and 2, whereas the entire set of chemical analyses are provided in the ESM Tables 1–8. Hereafter, we use the following abbreviations: K-fsp = alkali-feldspar, pl = plagioclase, cpx = clinopyroxene, ol = olivine, krs = kaersutite, mt = magnetite, ilm = ilmenite, bt = biotite, and ap = apatite. Temperature and pressure estimates (Table 3) are based on

Table 1 Petrographic description of trachytic pumices SB1 and SB3

Component/mineral phase	Size in mm	Volume %	Composition	Features
vesicles	Up to several tens	> 75		Elongated and coalescing Containing hawaiitic enclaves (SB3-ME)
pl	0.1–3.5	tr	$Or_{1–3}Ab_{32–43}An_{54–67}$	Anhedral Xenocrysts
K-fsp	0.1-4.0	tr	$Or_{19–37}Ab_{61–69}An_{2–12}$-homogeneous to slightly zoned	Euhedral to anhedral Some are rounded Resorbed cores Glomerules with cpx
cpx	0.1–0.4	tr	$Wo_{43–51}En_{33–43}Fs_{14–22}Mg\# = 63–77$ Normal and reverse zoned	Subhedral to anhedral Rounded and resorbed Xenocrysts Overgrowth of krs rims Aggregated with mgt, ilm, ap and K-fsp
amph	0.05–1.0	tr	kaersutite Ti = 0.5–0.8 apfu Si = 5.6–6.3 apfu Mg# = 65–77	Subhedral to anhedral Xenocrysts Rim around cpx
ol	0.1–0.3	tr	$Fo_{66–73}$ Normal zoned	Anhedral Xenocrysts Aggregated with ilm
bt	0.6–3.0	tr		Euhedral to anhedral
Fe–Ti oxides	0.05–1.5	tr	Usp = 0.50–0.56 mol Ilm = 0.89–0.90	Subhedral to anhedral rounded and dissolved Elongate skeletal and acicular growth, boxy cellular textures Ilm with ol mgt with cpx Inclusions of ap
ap	≤ 0.1	tr		Subhedral Inclusion in mgt and cpx

Single phenocrysts have an abundance of about < 1 vol% in SB1 and 2–5 vol% in SB3

pl plagioclase, *K-fsp* alkali-feldspar, *cpx* clinopyroxene, *amph* amphibole, *ol* olivine, *bt* biotite, *mgt* magnetite, *ilm* ilmenite, *ap* apatite, *krs* kaersutite, *tr* trace amounts (< 1%), *Mg# and Fo* $100 \times Mg/(Mg + Fe^{2+})$, *An* $Ca/(Ca + Na + K)$

Table 2 Petrographic description of hawaiitic enclaves SB3-ME

Component/mineral phase	Size in mm	Volume %	Composition	Features
Vesicles	0.01–0.1	~ 5		Circular and elongated Along crystal surfaces
pl	≤ 2	40–45	$Or_{0–13}Ab_{13–69}An_{22–87}$	Euhedral to anhedral Swallowtails shapes and skeletal growth Inter-grown with krs Aggregated with cpx, krs and mgt
cpx	0.1–0.3	10–15	$Wo_{42–50}En_{30–45}Fs_{12–23}$	Euhedral to anhedral Overgrown and inter-grown by krs
amph	≤ 0.15	20–25	kaersutite	Euhedral to anhedral Inter-grown with cpx
ol	≤ 0.15	< 5	$Fo_{73–82}$	Euhedral to anhedral
Fe–Ti oxides	≤ 0.4	< 5	mgt	Euhedral to anhedral, Elongate skeletal and acicular growth

Abbreviations as in Table 1

hypothetical equilibrium among pl, cpx and ol, and glass (e.g., Putirka 2008), between mineral pairs (e.g., K-fsp, pl, mgt - ilm; Bacon and Hirschmann 1988; Putirka 2008), or simply the composition of the mineral (e.g., amphibole; Ridolfi et al. 2010; Erdmann et al. 2014, for T estimates only).

White pumices (SB1)

White pumice clasts are fibrous, with spherical to elongated vesicles and feature a whitish-beige, silky shining, highly vesicular (> 75 vol%) glassy matrix (Table 1; Fig. 5a). They are mostly aphyric or with a low crystallinity (~ 1 vol%) composed of K-fsp, Fe–Ti oxides and bt. Vesicles are elongated and coalescing, reaching diameters of up to several centimeters. SB1 pumice clasts have a trachytic composition (~ 66.0 wt% SiO_2; ~12.6 wt% $Na_2O + K_2O$; Fig. 2a; ESM Table 1).

Banded pumices (SB3)

Banded pumice clasts have a highly vesicular groundmass, similar to the white pumices (SB1), but with a slightly higher crystallinity up to 2 vol%, and exhibit partly laminated brownish textures (Table 1; Fig. 5b, d). The groundmass contains sparsely distributed single phenocrysts (~ 2 vol%) of pl, K-fsp, cpx, krs, bt, mgt + ilm, ol, and ap. Mineral proportions are unclear, as the abundance is low. The brownish filaments contain mainly elongated microcrystals of Fe–Ti oxides and feldspars. Cpx and K-fsp have typically rounded shapes, and cpx is sometimes overgrown by krs. Ol is fragmented and mgt shows skeletal growth. SB3 pumice clasts are trachytic in composition with relatively low SiO_2 content (~ 62.4 wt%; ~12.0 wt% $Na_2O + K_2O$; Fig. 2a; ESM 1; Queiroz et al. 2015). Another characteristic feature is the occurrence of mafic enclaves (SB3-ME) with sharp contact and cuspate margins (i.e., a pointed end, where two curves meet) with the surrounding groundmass glass (Fig. 5d).

Table 3 Calculated H_2O_{melt} contents, temperatures, pressures and oxygen fugacities after thermobarometers for feldspar (fsp)-liquid pairs, amphibole (amph) and olivine (ol)-liquid pairs

Sample	H_2O_{melt} in wt%	T in °C		
	Fsp-liq[b]	Fsp-liq[b]	Ol-liq[a]	Amph[c]
	Eq. 25b SEE ± 1.1	Eq. 24a SEE ± 36	Eq. 22 SEE ± 43	SEE ± 22
SB1	3.61–5.68	870–901	–	–
SB3-ME	0.34–5.00	866–1012	1057–1142	982–1007

[a]Putirka et al. 2007

[b]Putirka 2008

[c]Ridolfi et al. 2010

Mafic enclaves (SB3-ME)

Mafic enclaves (ME) have diktytaxitic texture and are composed of pl (40–45 vol%), krs (20–25 vol%), cpx (10–15 vol%), mgt (~ 5 vol%), ol (< 5 vol%), and vesicles (~ 5 vol%; Table 2; Figs. 5e–g, 6a). The glassy groundmass (≤ 2 vol%) is not clearly distinguishable from pl, but is identified by the occurrence of spherical vesicles. A notable feature is that the ME show fast cooling textures like sharp contacts with the surrounding trachytic groundmass, and mineral phases connote fast growing crystal textures such as acicular shapes, boxy cellular features, swallowtails, and skeletal textures (Figs. 5e–g, 6a). SB3-ME has a hawaiitic composition, with ~49 wt% SiO_2 and ~6.1 wt% $Na_2O + K_2O$ (Fig. 2a; ESM 1).

Feldspars

Alkali-feldspar occurs as euhedral-to-anhedral anortho-clase ($Or_{19–36}$; Figs. 6g, 7c) in SB1 and SB3 trachytic pumice clasts, whereby SB3 also contains some pl (labradorite; $An_{54–67}$). hawaiitic enclaves (SB3-ME) contain pl, as mainly bytownite to andesine and a few oligoclase ($An_{22–86}$). K-fsp in SB3 is homogeneous to slightly zoned, features rounded crystal shapes and resorbed cores (Figs. 5h, 6g) and are, therefore, considered to be xenocrysts. Some K-fsp in SB3 forms glomerules in association with cpx. Pl in SB3-ME is euhedral to anhedral and aggregated with cpx, krs, and mgt (Fig. 6a). It often exhibits acicular, swallowtail shapes, and skeletal growth (Fig. 5e–g).

Clinopyroxene

Clinopyroxene occurs in the trachytic groundmass of SB1 and SB3 as diopside and augite with mainly rounded and resorbed shapes (Fig. 6b, c). It is characterized by Mg# ranging from 63 to 77 [Mg# $= (100 \times Mg/(Mg + Fe^{2+}))$] and can be considered as a xenocryst out of equilibrium with MgO–poor host rock. Cpx is often aggregated with ap, mgt, and ilm and sometimes with K-fsp. Some crystals display thin krs rims (Fig. 6b). Cpx in hawaiitic SB3-ME is also diopside and augite (Mg# = 57–78, Fig. 7a, b), and is often overgrown by krs (Fig. 6a). Al_2O_3 and TiO_2 contents roughly decrease with high Mg# in cpx from the hawaiitic enclaves (Fig. 7a, b).

Amphibole

Amphibole is present as euhedral to subhedral krs [Mg# = 65–77], in the groundmass of SB1 and SB3 (Fig. 6c, f), and as rims around cpx in SB3 (Fig. 6b). Krs in hawaiitic SB3-ME ranges from euhedral to anhedral, compositionally equal to krs in the trachytic groundmass,

Fig. 5 Photographs of eruptive products from the Santa Bárbara Formation showing **a** white pumice clast, representing the felsic end-member SB1, **b** banded pumice clasts from SB3, **c** lava from a dyke in the inner caldera wall of the western flank, representing the mafic end-member SC-MD, **d** thin section photomicrograph of SB3 illustrating the mafic enclaves (SB3-ME), brownish filaments (SB3-A) and the light-colored groundmass (SB3-B). **e–g** Photomicrographs of mafic enclaves (SB3-ME) that are mainly composed of plagioclase, kaersutite and magnetite with quenching textures shown by sharp contacts between crystals and trachytic groundmass, by skeletal and acicular mgt and pl crystals and **g** pl with swallowtail. **h** Alkali-feldspar with resorbed core in trachytic groundmass of SB3. *mgt* Magnetite, *pl* plagioclase, *K-fsp* alkali-feldspar, *krs* kaersutite
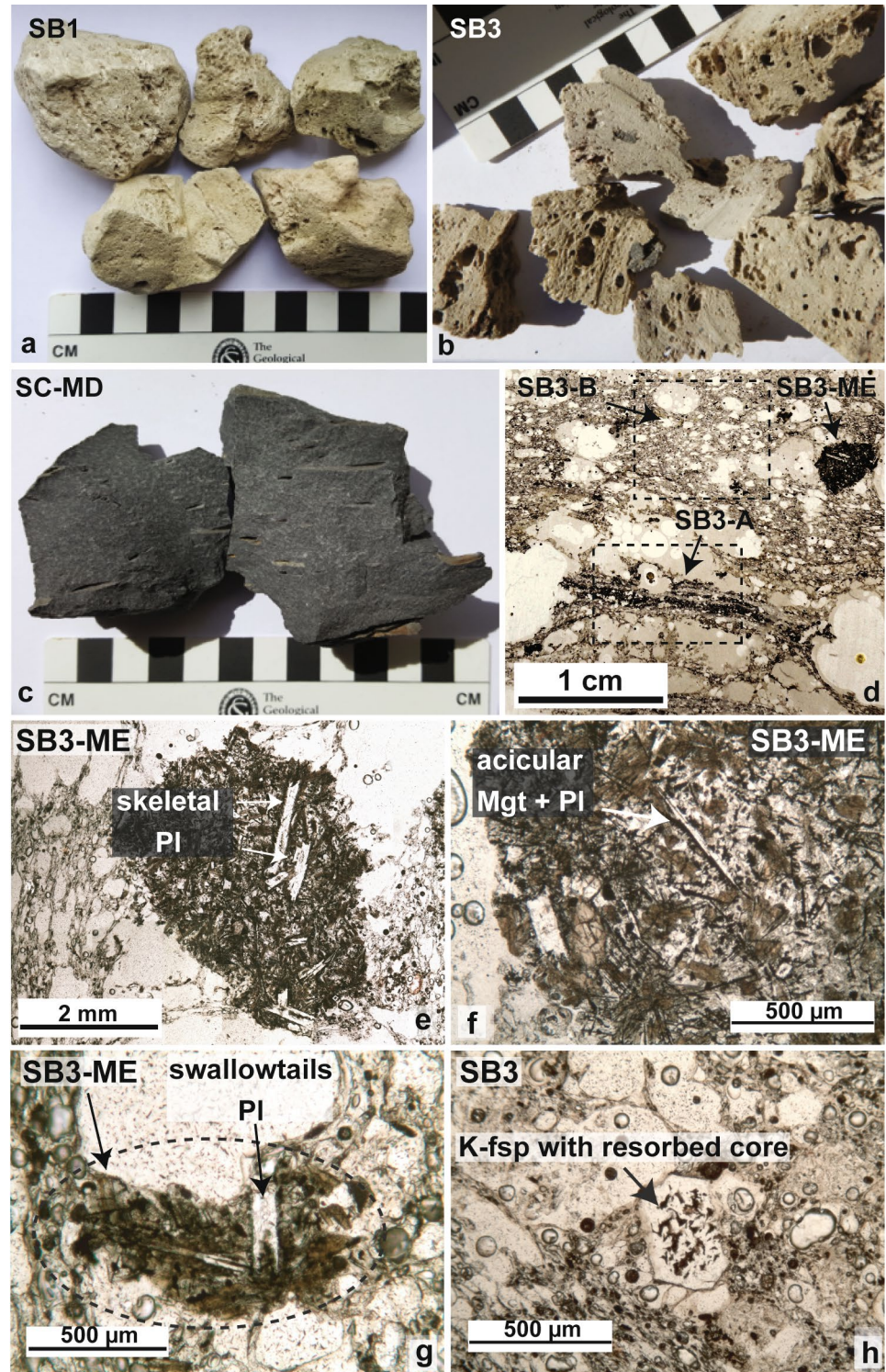

and sometimes is inter-grown with cpx (Fig. 6a). Many krs in SB3 groundmass do not follow the stability test suggested by Ridolfi et al. (2010), and therefore, have been discarded for thermometric estimations.

Olivine

Olivine occurs as subhedral to anhedral crystals in SB3 with normal zoning by $Fo_{66–73}$ and is sometimes grown together

Fig. 6 BSE images of SB3 samples. **a** Paragenesis of pl, cpx, krs, and mgt in mafic enclaves. Note mgt with elongated and boxy cellular growing textures, krs has skeletal textures that is sometimes inter-grown with cpx. Interstitial glass is clearly visible with spherical vesicles. **b** Dissolved oscillatory zoned cpx in trachytic groundmass shows rims of krs. **c** Dissolved, normal zoned ol aggregated with ilm, dissolved and reverse zoned cpx in groundmass. **d** Mgt with skeletal growth and **e** with rounded crystal shapes, embayments and inclusions of ap. **f** Euhedral krs and skeletal grown mgt in groundmass. **g** Anhedral homogeneous K-fsp in groundmass. *K-fsp* Alkalifeldspar, *pl* plagioclase, *cpx* clinopyroxene, *ol* olivine, *fo* forsterite, *amph* amphibole, *krs*, kaersutite, *mgt* magnetite, *ilm* ilmenite, *ap* apatite
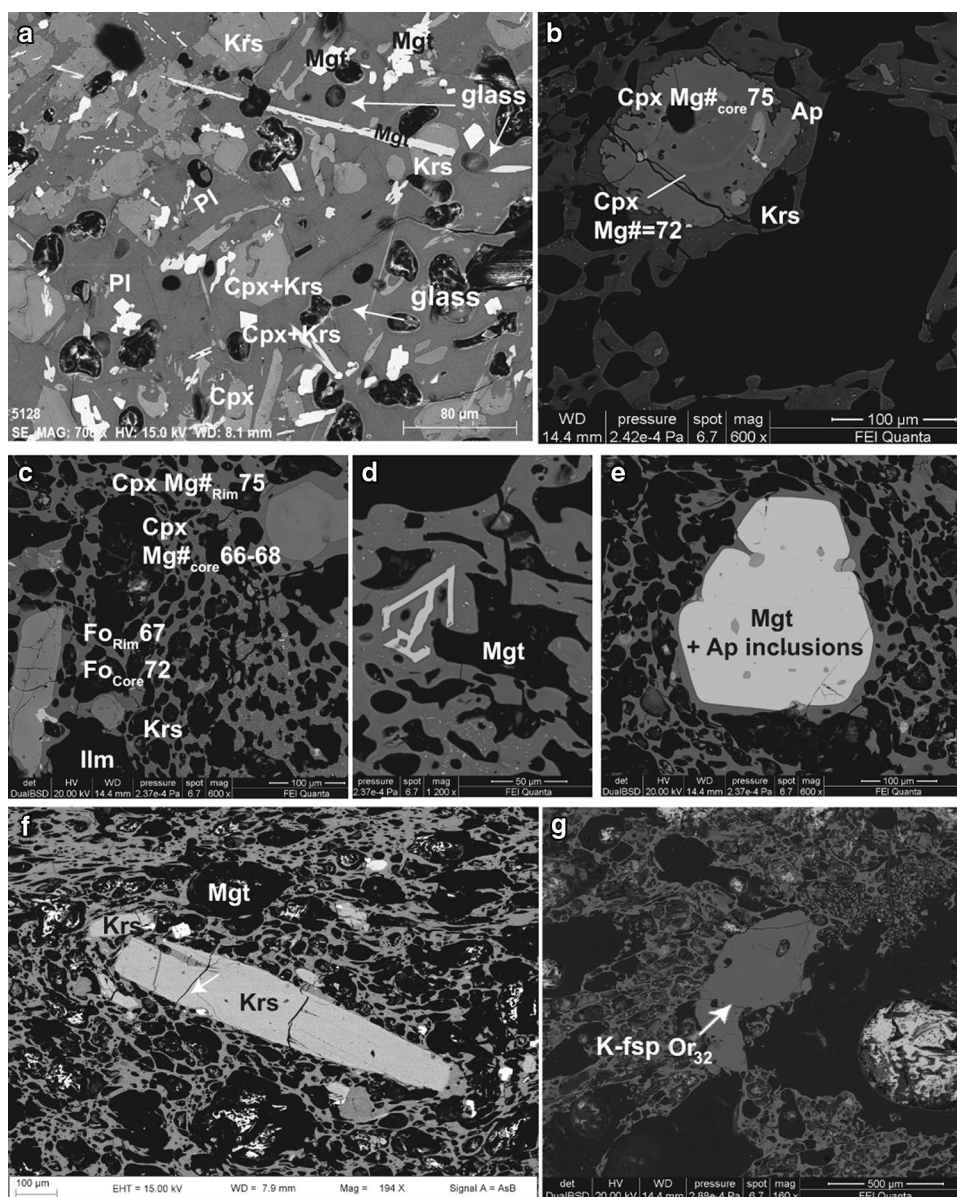
with ilm (Fig. 6c). Ol occurring in the hawaiitic SB3-ME is euhedral to anhedral and ranges from Fo_{73} to Fo_{82}.

Fe–Ti oxides

Magnetite crystals are homogeneous, subhedral to anhedral, rounded and dissolved, and occurs both in the trachytic groundmass of SB1 and SB3 (Fig. 6d–f) and hawaiitic SB3-ME (Fig. 6a). Rhombohedral phases are ilm-rich (ilm = 0.89–0.90) and are present in the trachytes only, sometimes aggregated with ol (Fig. 6c). Few coexisting mgt and ilm fulfill the equilibrium test of Bacon and Hirschmann (1988). Mgt in trachytic groundmass is aggregated with cpx and occasionally contains ap. Crystals show elongated,

skeletal and acicular growth, and boxy cellular textures (Fig. 6a, d–f).

Glass compositions from Santa Bárbara products

Overall, the trachytic groundmass glass of banded pumices (SB3) shows decrease of TiO_2, FeO, MgO (Mg#), and CaO with increasing SiO_2 (Figs. 2b–e, 8c–f). However, the trachytic glasses are characterized by slight differences that allow for the distinction of two trends within the same sample, represented by SB3-A and SB3-B (Fig. 8), where SB3-A coincides optically with darker bands and SB3-B with light-colored areas (Fig. 5d). SB3-A glass ranges from 60.3 to 66.6 wt% SiO_2 and SB3-B from 63.0 to 65.6 wt% SiO_2. The main difference is that SB3-B glass has lower contents
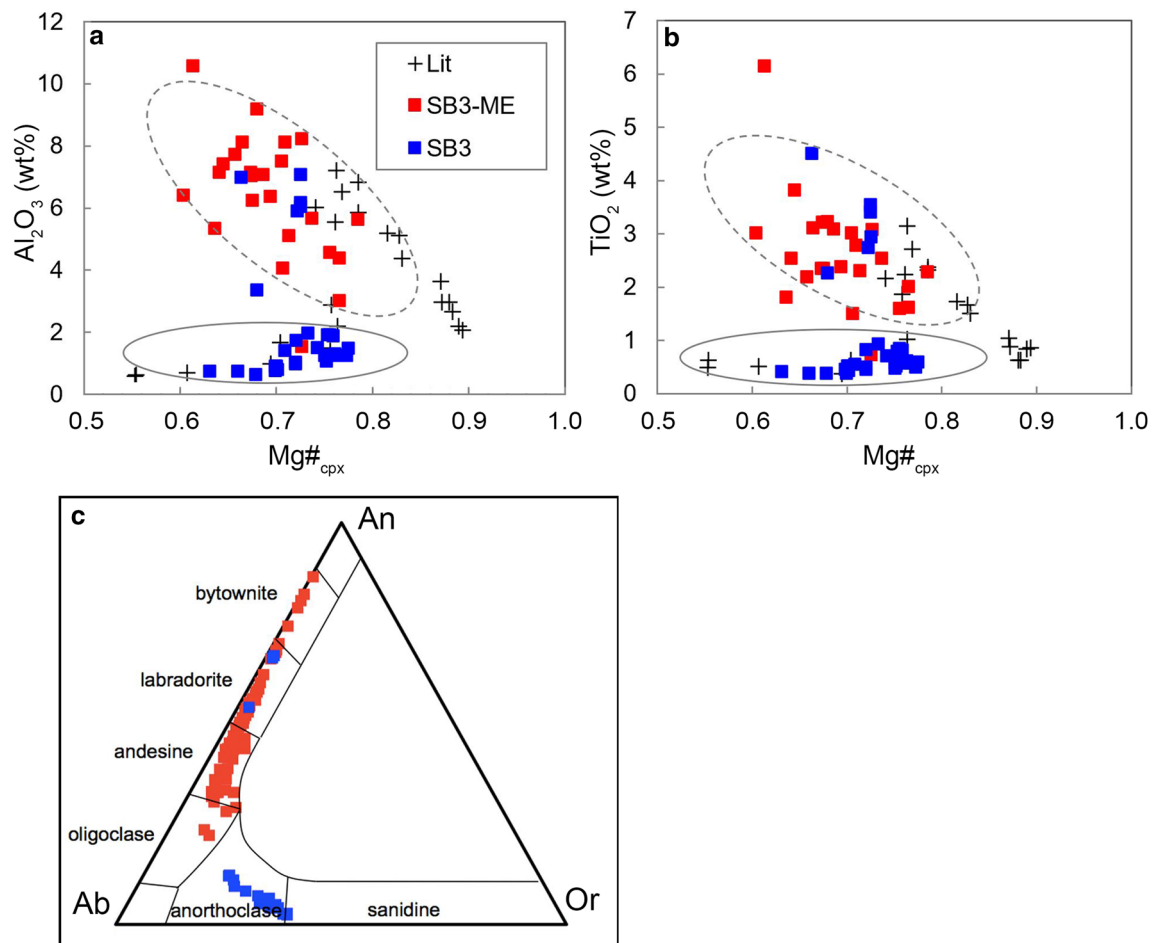
Fig. 7 Chemical distinction between **a, b** clinopyroxene and **c** feldspar in SB3 samples. Blue color displays minerals in the trachyte (SB3) and red colors in the hawaiite (SB3-ME). Clinopyroxene compositions are expanded by clinopyroxene compositions from hawaiites to trachytes after Renzulli and Santi (2000) and Beier et al. (2006). Dashed line includes high-pressure and continuous line low-pressure-derived clinopyroxene (Beier et al. 2006)

of TiO_2, FeO (neither shown), MgO, and CaO, and higher amounts of Al_2O_3 and Na_2O than SB3-A at similar SiO_2 concentrations. SB3-A can be distinguished from SB3-B also, because it has almost constant Al_2O_3 and Na_2O contents, while in SB3-B, these oxides decrease with increasing SiO_2. The interstitial glass in the hawaiitic enclaves (SB3-ME glass, 62.9–64.4 wt% SiO_2) is chemically indistinguishable from SB3-B glass (Fig. 8).

Thermobarometry

Temperatures of natural samples were calculated using crystal-liquid pairs (crystal rim−matrix glasses) for feldspar–liquid, olivine–liquid pairs (Putirka et al. 2007; Putirka 2008) and amphibole thermometry (Ridolfi et al. 2010). All crystallization conditions are summarized in Table 3. A detailed description and application of geothermobarometers on mineral and melt compositions is provided in the

Electronic Supplementary Material. Results indicate temperatures of 870–901 °C for the trachytic magma with a water content of 4–6 wt% and 1057–1142 °C (olivine crystallization), 982–1007 °C (amphibole crystallization), and 866–1012 °C (0.3–5 wt% H_2O_{melt}; plagioclase crystallization) for the hawaiitic magma that crystallized at a depth of ~ 10.5–13 km.

Discussion

Crystallization conditions of the Santa Bárbara products

Concerning the hawaiitic magma (SB3-ME), ol-liq ($Fo_{~73}$), krs, and fsp-liq geothermometers yield crystallization temperatures (T) of about 1101 ± 39 °C, 985 ± 20 °C, and 936 ± 55 °C, respectively (Table 3). Eventually, the hawaiitic

Fig. 8 Selected major elements versus silica in groundmass glasses of Santa Bárbara products (**a**–**h**): glass compositions (circles), whole-rock composition of the mafic enclaves (squares), and the mafic and felsic end-members used for time-series experiments (diamonds). Diagrams on the right-hand side show only the more evolved compositions. All compositions are normalized to 100%
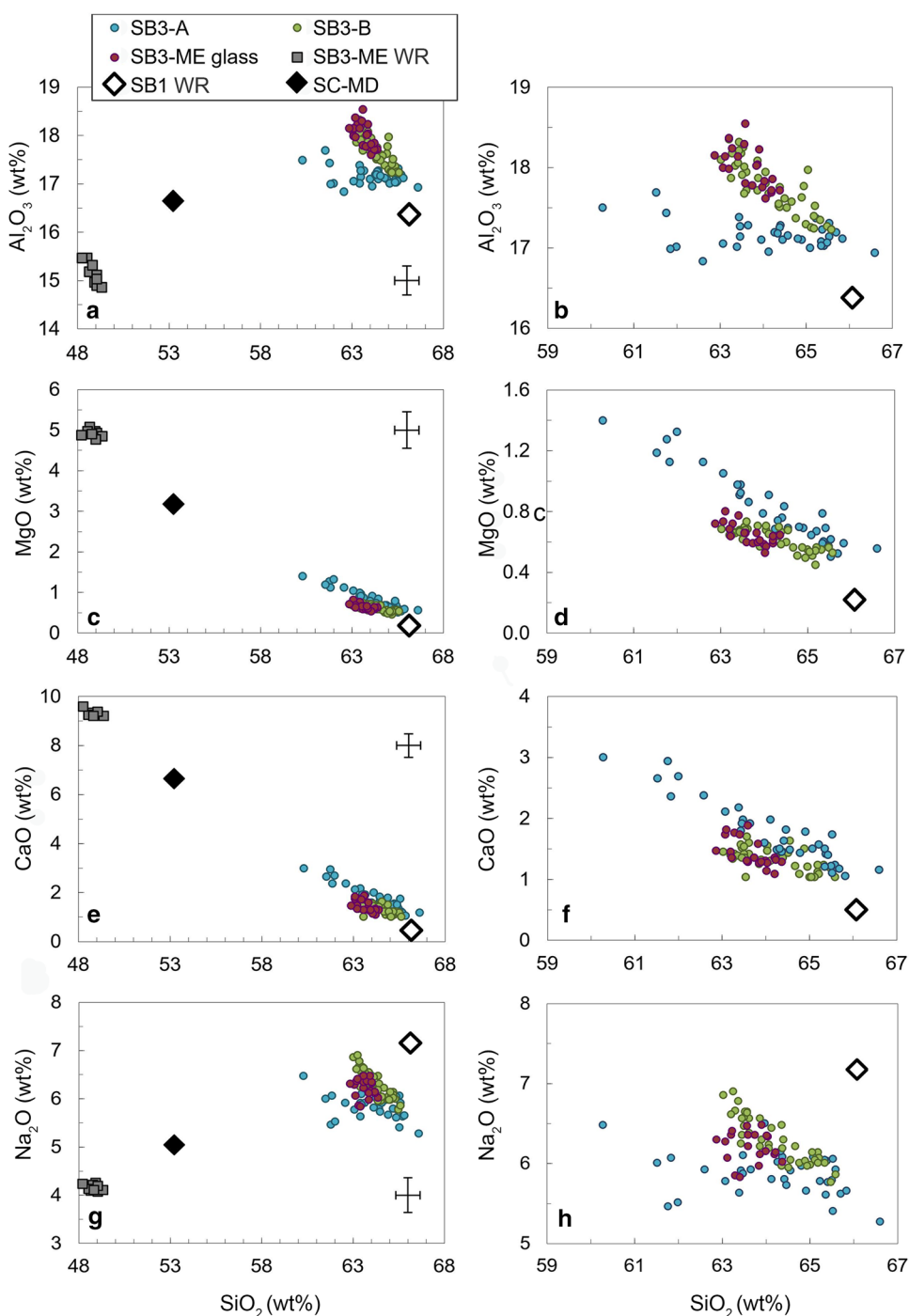

magma crystallized at a depth of ~ 10–13 km (Renzulli and Santi 2000; Beier et al. 2006) and was later quenched during intrusion and mingling in the trachytic magma reservoir (Paredes-Mariño et al. 2017; Porreca et al. 2018) at shallow depth of ~ 3–4 km (Beier et al. 2006). Crystallization temperatures of the mafic magma modeled by Paredes-Mariño et al. (2017) are in agreement with our results.

The trachytic magma (SB1) represents the most evolved composition (MgO < 0.3 wt%, Figs. 2, 8, 9). In this case,

pressure (P) estimations could not be obtained as only K-fsp and mgt-ilm pairs fulfill equilibrium tests. Nevertheless, calculated T and H_2O_{melt} contents of the trachyte are ~ 870–884 °C and 3.6–5.8 wt%, respectively (Table 3). It is proposed that the trachytic composition was generated by stagnation and fractional crystallization of hawaiitic magma at depth (Mattioli et al. 1997; Renzulli and Santi 2000) and subsequent melt segregation to shallower levels. A similar process can be proposed for

Fig. 9 Major element compositions of glasses from mixing experiments EXP1 (blue), EXP2 (red) and EXP3 (beige). White and black represent the mafic and the felsic end-member, respectively. Except for Na$_2$O and K$_2$O, the experiments correlate well with the groundmass glasses of SB3-A. All compositions are normalized to 100%
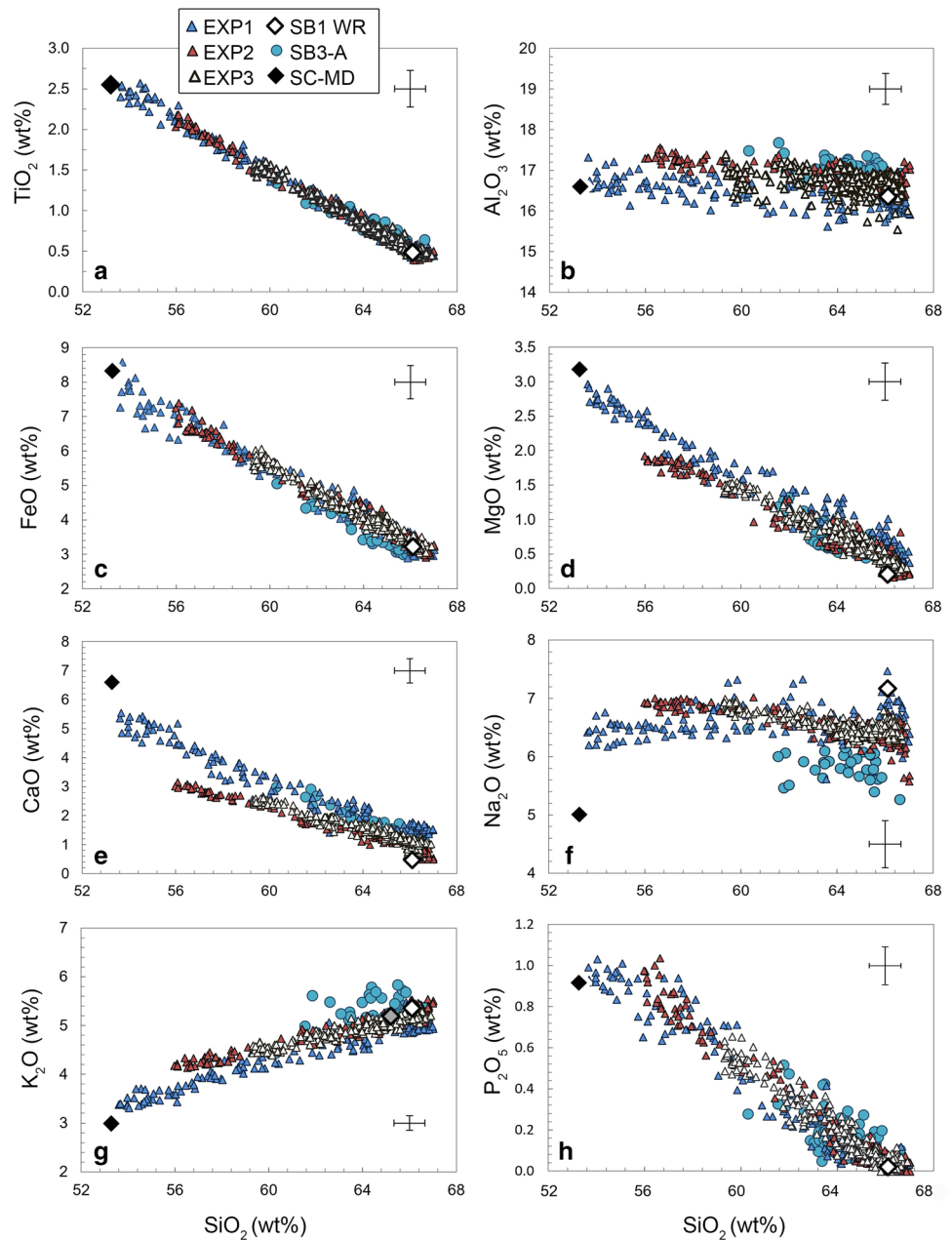
the trachytic interstitial glass of the hawaiitic enclaves (SB3-ME glass) that is chemically indistinguishable from the groundmass glass SB3-B (Fig. 8). Instead, SB3-A groundmass glass is allocated to an incomplete mixing event (mingling), as it coincides petrographically and compositionally with stretching and folding textures (i.e., the brownish filaments) observed in sample SB3 and in magma-mixing experiments (Figs. 4, 5c, 8; Perugini et al. 2004). Pimentel et al. (2015) reported similar observations for the banded pumice clasts of the C11 deposit of Caldeira Volcano (Faial, Azores). Ol crystals of SB3 hint to a putative melt composition of

Mg# = 34–47 [K_D(Fe–Mg)$_{ol–liq}$=0.30 ± 0.03; Roeder and Emslie 1970; Rhodes et al. 1979; Putirka 2008], while cpx xenocrysts indicate equilibrium with a melt with ~Mg# = 26–47 [K_D(Fe–Mg)$_{cpx–liq}$ at 900 °C=0.21 ± 0.08; K_D(Fe–Mg)$_{cpx–liq}$ at 1100 °C=0.26 ± 0.08; Putirka 2008]. Following the Mg# trend of SCV magmas (Fig. 2d), the equivalent host magma of ol and cpx plots between ~48–64 wt% SiO$_2$ (hawaiite to trachyte) indicating a wide range in composition. This magma composition that is highly probable the mafic end-member has led to the banded textures in sample SB3, shown by the SB3-A groundmass glasses (Figs. 5c, 8).

Constraints from time-series mixing experiments

To better constrain the above-mentioned magma-mixing process, we performed magma-mixing experiments between a mugearitic lava (SC-MD) from SCV and sample SB1 (Fig. 4; ESM Table 8). The degree of mixing (homogenization and diffusion) increases with time, which is optically seen by a higher abundance of finer filaments with increasing run time of the experiments. Initially, contacts between the end-members are sharp and oscillating, as in the ~10.5 h experiment (EXP1) and develop later to visually indistinguishable smooth filaments of μm-scale size (EXP2 and EXP3; Fig. 4). The compositional ranges converge towards the felsic end-member, narrowing the hybrid composition and the mafic end-member disappears with time (Fig. 9; all major element oxides normalized to 100%, on water-free basis).

Overall, all the major oxides define a linear mixing trend between the two end-members (SC-MD and SB1) that substantially covers the compositional patterns of SB3-A glasses. Na$_2$O and K$_2$O constitute exceptions (Fig. 9f, g). Na$_2$O is the fastest moving major element due to a high diffusion coefficient (Watson and Jurewicz 1984; Baker 1990, 1991), this is shown by a rapid homogenization towards the hybrid compositions shortly after the start of the experiments (Fig. 9f). Immediately after mixing starts, the melt of the mafic component enriches rapidly in Na$_2$O (~6.5 wt% Na$_2$O at ~54 wt% SiO$_2$). Besides, Na$_2$O illustrates a nonlinear undulating variation between the end-members with lower sodium contents at higher silica contents, for the 21 h and 42 h experiments (EXP2 and EXP3, respectively). This is explained by the slower diffusion of network formers, such as Si, than network modifiers (e.g., Na), resulting in gradients in the chemical potential of the faster elements. As a consequence, the net flux of Na$_2$O changes direction to neutralize the chemical potential (e.g., Watson 1982; Watson and Jurewicz 1984) and finally forms a valley at high SiO$_2$ contents. In comparison with the experimental compositions, Na$_2$O is depleted in the natural sample. In this case, it could be explained by feldspar crystallization, but this trend is not visible within other major elements, such as Al$_2$O$_3$ or CaO. On closer inspection, Al$_2$O$_3$ also behaves divergently,

as it scatters strongly, although the starting concentrations are not significantly different (Fig. 9b, 16.4–16.7 wt%). This can be explained simply by limits of reproducibility of the data related to a small compositional range. Another process potentially leading to Na$_2$O depletion in natural samples is the strong coupling between alkalis and Al activities, especially occurring for alkali concentrations above 8 wt% (Guo and Zhang 2016; González-García et al. 2017). Except the particular behavior of Na, the compositional element signature of the trachytic SB3-A glasses is well reproduced by our experiments (Figs. 8, 9).

As a subsequent step, we calculate timescales of mixing using the concentration variance decay (CVD; Perugini et al. 2015) for SB3-A. The CVD displays the degree of homogenization during mixing of compositionally different components with proceeding time and can be calibrated from time-series experiments (Morgavi et al. 2013a, b; Perugini et al. 2013, 2015; Rossi et al. 2017). We quantified the concentration variance $\sigma^2(C_i)$ for each major element (i) between the starting compositions SB1 and SC-MD at time $t = 0$ and at all experimental durations ($t = ~10.5, 21,$ and 42 h) to determine the normalized concentration variance $\left(\sigma_n^2\right)$ following the equation:

$$\sigma_n^2(C_i) = \frac{\sigma^2(C_i)t}{\sigma^2(C_i)t = 0}. \tag{3}$$

Equally, we estimated $\sigma_n^2(C_i)$ for the compositions of SB3-A groundmass glass using also the variance between the end-member compositions of SB1 and SC-MD as the initial variance. As the next step, the CVD was calculated on the basis of the experiments using the following exponential function:

$$\sigma_n^2(C_i) = C_0 e^{(-Rt)}, \tag{4}$$

where $R = $ CVD and C_0 is the normalized variance at $t = 0$. R was determined via orthogonal fitting using Python (Oliphant 2007). The statistical robustness of the proposed approach has been estimated by Rossi et al. (2017), and results highlight that these empirical relationships remain valid by removing up to 80% of the analytical determinations. We neglected CVD calculations of Al$_2$O$_3$ and Na$_2$O,

Table 4 Calculated fitting parameter (C_0, R) used to fit the concentration variance decay for samples EXP1-3 and used to estimate the mixing to eruption time for sample SB3

| Element species | Fitting parameters | | | | Normalized variance σ_n^2 | | | | Time (h) |
	C_0	stdev	R	stdev	EXP1	EXP2	EXP3	SB3-A	SB3-A
SiO$_2$	0.97	0.08	0.08	0.01	0.38	0.25	0.11	0.05	36.3
TiO$_2$	0.97	0.08	0.08	0.01	0.38	0.25	0.10	0.03	40.6
FeO	0.97	0.14	0.10	0.02	0.31	0.20	0.09	0.04	31.2
MgO	0.99	0.13	0.13	0.02	0.24	0.12	0.06	0.03	27.7
CaO	0.99	0.06	0.16	0.01	0.18	0.05	0.02	0.03	21.9
K$_2$O	0.98	0.09	0.14	0.01	0.22	0.09	0.04	0.07	19.0

because end-members have similar Al_2O_3 concentrations, and Na_2O is strongly controlled by other diffusion related effects (see above). The 42 h experiment (EXP3) gives a higher concentration variance (σ_n^2, Eq. 3) of SiO_2, TiO_2, FeO, and MgO, compared to equivalent elements in SB3-A glasses, whereas σ_n^2 of CaO and K_2O is lower (Table 4). This indicates that the degree of homogenization of the aforementioned elements is lower compared to the natural glasses, whereas the degree of homogenization of CaO and K_2O is higher in the experiments. This is attributed to the complex character of natural glasses, where other processes than the only magma mixing occur (Morgavi et al. 2013a, 20013b).

For this reason, we fitted the CVD (Eq. 4) of each element for the duration of the experiments (Fig. 10). The highest CVD is given by CaO with 0.16 and the lowest being 0.08 (SiO_2 and TiO_2; Table 4). The high deviation is due to varying mobility of these chemical elements, reflecting the high mobility of K as a network modifier (e.g., Watson 1982; Watson and Jurewicz 1984) and the slow diffusion character of Si and Ti, as network-forming species, respectively. CVD of FeO, MgO or CaO lie in between. These elements are considered to diffuse faster in felsic melts, compared to mafic melts. However, on the basis of the fitted parameters R (CVD) and C_0 for each element, we quantified the mixing time for SB3-A glasses. Calculations indicate that the time of mixing ranges from around 19.0–40.6 h for K_2O and TiO_2, respectively (Table 4). These results suggest a magma-mixing event that occurred between 0.8 and 1.7 days before the eruption. The dark filaments in the groundmass and their chemical composition (SB3-A) point to an incomplete mixing event that was finally frozen by the eruption. To better understand, we would like to stress that the calculated mixing times aim to constrain the period between the

beginning of the magma-mixing process and the onset of the eruptive event. This is because our modelling assumes that the syn-eruptive chemical diffusion is negligible, due to the fast decrease of temperature during the magma ascent, resulting in the freezing of the variance decay process. We consider these results as valid when compared with experimental studies, where mixing timescales for other volcanic eruptions have been calculated (Kouchi and Sunagawa 1983, 1985; Morgavi et al. 2013a, b; Perugini et al. 2013, 2015; Laumonier et al. 2015). Rossi et al. (2017) conducted an experimental investigation on the relationship between Reynolds numbers (*Re*) and homogenization timescales (see the section titled "Scaling of the experiments to natural scenarios" for further details). They determined that when mixing events take place a few hours before an eruption, with a $Re \sim 10^{-9}$, it will result in filaments with mm to µm width, as seen in SB3, where the filaments range from 4 to 200 µm. According to this, and in agreement with our calculated timescales, Re would be close to 10^{-10}.

Inferring the pre-eruptive plumbing system dynamics of the Santa Bárbara eruption

Deciphering the dynamics occurring in a volcanic plumbing system before an eruption is always a challenging task. We suggest that the SB eruptive products represent a trachytic magma reservoir located within the oceanic crust (Fig. 11) that evolved by fractional crystallization from a hawaiitic parental magma. To explain the origin of a trachyte containing hawaiitic enclaves, two hypotheses are proposed. The first hypothesis is that xenocrysts of pl, cpx, ol, krs, and mgt record at least one former replenishment of the SCV trachytic reservoir ~ 19–41 h before the eruption by a mafic magma with hawaiite-to-benmoreite composition (Fig. 11a). The banded textures of SB3-A groundmass glass are, therefore, the product of magma mixing between the resident trachyte and the hawaiite/benmoreite intrusion. This intrusion caused the thermal destabilization of the SCV magmatic system. The trachytic magma reservoir was intruded a second time by another hawaiitic magma, represented by the hawaiitic enclaves, that enhanced convection. We suggest that the new magma was volatile-rich (≤ 5 wt% H_2O), hot (~ 1100 °C; Fig. 11b) and strongly undercooled when in contact with the trachyte. In addition, we propose, in agreement with Paredes-Mariño et al. (2017) and Porreca et al. (2018), that bubble nucleation increased the internal pressure of the reservoir, which triggered the SB eruption. In detail, Paredes-Mariño et al. (2017) proposed a trachytic magma reservoir at depth of 3.5–4.0 km with T of 990 °C and ~ 2 wt% H_2O, and a hawaiitic magma with T of 1160 °C at the moment of mingling between the two magmas. Our calculations point to a higher T gradient
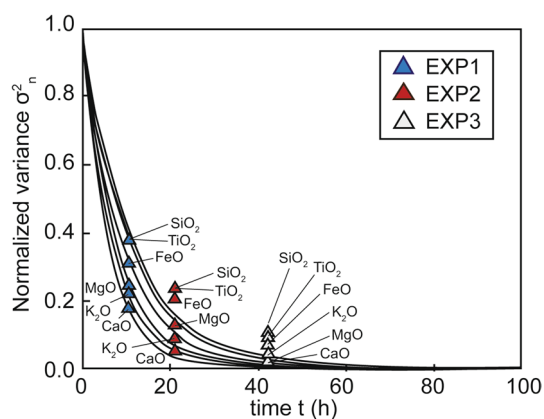
Fig. 10 Normalized concentration variance against time for selected major elements of the mixing experiments indicating the exponential decay of the concentration variance (CVD, continuous line). From top to bottom, the curves illustrate the CVD for SiO_2, TiO_2, FeO, MgO, K_2O and CaO
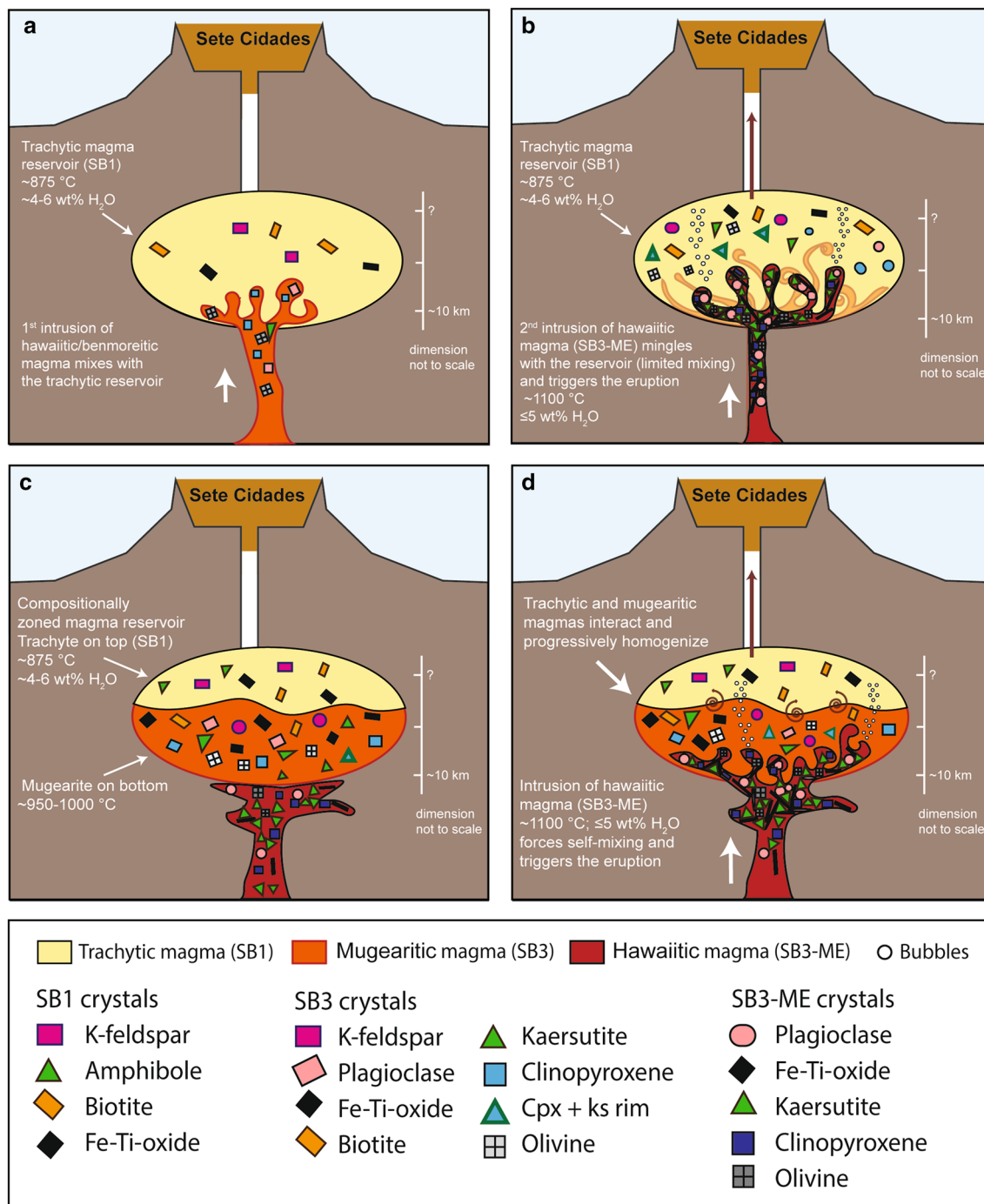
Fig. 11 Schematic model of the Sete Cidades Volcano prior to the Santa Bárbara eruption, showing the two hypotheses. Hypothesis I: **a** intrusion of a hawaiitic/benmoreitic magma into the trachytic reservoir leads to the mixing between the two magmas and destabilization of the reservoir ~ 19–41 h before the onset of the eruption. Remnants of the intrusion are plagioclase, clinopyroxene and olivine. **b** Second intrusion of hawaiitic magma, recorded by the mafic enclaves, mingles with the unstable reservoir, triggering the eruption. Hypothesis II: **c, d** Compositionally zoned magma reservoir, from trachyte on top to mugearite on the bottom, is intruded by a hawaiitic magma that mingles with the resident magma and destabilizes the reservoir, triggering the eruption ~ 19–41 h afterward

between the trachytic and hawaiitic magmas, which is not necessarily in disagreement, as the trachytic reservoir was reheated by the previous intrusions. The calculated lower T is more likely linked to crystallization in an upper colder level of the reservoir, where sample SB1 was generated. Nonetheless, the first replenishment of the

reservoir with hawaiitic magma resulted in a T increase that most probably caused the dissolution of various mineral phases in the trachytic magma.

The second hypothesis is that the SCV magma reservoir was compositionally zoned prior to the SB eruption, with trachyte on the top and mugearite at the bottom, from where pl, cpx, krs, and ol derive (Fig. 11c, d). Compositionally zoned magma reservoirs are commonly reported for other magmatic systems of the Azores, including Fogo and Furnas volcanoes (São Miguel) and Pico Alto Volcano (Terceira; e.g., Snyder et al. 2007; Jeffery et al. 2016; D'Oriano et al. 2017). The intrusion of a hot hawaiitic magma from depth might have induced thermo-chemical instability in the compositionally zoned reservoir. The contact between the hot mafic magma and the colder felsic one, caused under-cooling of the uppermost layer of hawaiitic magma, the latter found as hawaiitic enclaves in the erupted products. The progressive cooling and crystallization of the hawaiitic magma induced the exsolution of the volatile phase, which, due to density difference, separated from the hawaiitic liquid and moved upward through the zoned reservoir. Bubble ascent dynamics through the zoned reservoir potentially enhanced the mixing process in agreement with the experimental results reported by Wiesmaier et al. (2015). Due to the combined effects of thermal instability and volatile exsolution, the zoned reservoir became unstable developing convective dynamics, and this triggered the mixing between the mugearitic and the trachytic magmas (e.g., Cardoso and Woods 1999; Snyder 2000).

The presence of disequilibrium textures in crystals and oscillatory zoning in cpx can also be indicators of convection within the system, as crystals that are previously in equilibrium with the felsic liquid were forced to interact with a more mafic magma. Growth rims of krs around cpx indicate the interaction of the cpx crystals with H_2O-rich magmas. This evidence is also in favor of convective dynamics within the reservoir, moving the cpx crystals within regions of variable water contents. The combined effect of thermodynamic destabilization of the reservoir and the overpressure generated by exsolution of volatiles was probably the trigger of the SB eruption (Paredes-Mariño et al. 2017; Porreca et al. 2018). We suggest that the second hypothesis provides the best explanation for the observed features in the studied samples. A possible scenario is that the intrusion of the mafic magma into a vertically zoned evolved magma reservoir took place ~ 19–41 h before the onset of the eruption. In addition, as proposed by Paredes-Mariño et al. (2017), the fragments of hawaiitic enclaves possibly served as favorable sites for bubble nucleation and growth, enhancing the explosivity of the eruption.

Conclusions

The products of the 16 ka Santa Bárbara Formation (Sete Cidades Volcano) were investigated to unravel its pre-eruptive magma storage conditions. We combined mineralogical observations, geochemical modeling, petrological considerations, and experimental simulations of magma mixing to provide a clearer picture of the Sete Cidades plumbing system before Santa Bárbara eruption. The several phenocryst populations of the Santa Bárbara trachytic magma result from changes in composition and P–T conditions that were most likely due to self-mixing event after hawaiite intrusion and convection in the reservoir. We emphasize that the eruption was triggered by the injection of hawaiitic magma, represented by the mafic enclaves in the pumice clasts, producing volatile exsolution and a subsequent reservoir overpressure. Overall, our findings fill the gap of missing geochemical and petrological investigations about the Santa Bárbara Formation and show that magma mixing is a key process leading to paroxysmal explosive eruptions of Sete Cidades Volcano.

References

Bacon CR, Hirschmann MM (1988) Mg/Mn partitioning as a test for equilibrium between coexisting Fe–Ti oxides. Am Mineral 73:57–61

Baker DR (1990) Chemical interdiffusion of dacite and rhyolite: anhydrous measurements at 1 atm and 10 kbar, application of transition state theory, and diffusion in zoned magma chambers. Contrib Mineral Petrol 104:407–423

Baker DR (1991) Interdiffusion of hydrous dacitic and rhyolitic melts and the efficacy of rhyolite contamination of dacitic enclaves. Contrib Mineral Petrol 106:462–473

Beier C, Haase KM, Hansteen TH (2006) Magma evolution of the Sete Cidades Volcano, Sao Miguel, Azores. J Petrol 47:1375–1411

Booth B, Croasdale R, Walker GPL (1978) A quantitative study of five thousand years of volcanism on São Miguel, Azores. Philos Trans R Soc A 288:271–319

Cardoso SSS, Woods AW (1999) On convection in a volatile-saturated magma. Earth Planet Sci Lett 168:301–310

Cole PD, Pacheco JM, Gunasekera R, Queiroz G, Gonçalves P, Gaspar JL (2008) Contrasting styles of explosive eruption at Sete Cidades, São Miguel, Azores, in the last 5000 years: hazard implications from modeling. J Volcanol Geotherm Res 178:574–591

D'Oriano C, Landi P, Pimentel A, Zanon V (2017) Magmatic processes revealed by anorthoclase textures and trace element modeling: the case of the Lajes Ignimbrite eruption (Terceira Island, Azores). J Volcanol Geotherm Res 347:44–63

Erdmann S, Martel C, Pichavant M, Kushnir A (2014) Amphibole as an archivist of magmatic crystallization conditions: problems, potential, and implications for inferring magma storage prior to the paroxysmal 2010 eruption of Mount Merapi, Indonesia. Contrib Mineral Petrol 167:1–23

Escartín J, Cannat M, Pouliquen G, Rabain A (2001) Crustal thickness of V-shaped ridges south of the Azores: interaction of the Mid-Atlantic Ridge (36–39 N) and the Azores hot spot. J Geophys Res 106:719–721

Galaktionov OS, Anderson PD, Peters GWM, Meijer HEH (2002) Mapping approach for 3D laminar mixing simulations: application to industrial flows. Int J Numer Methods Fluids 40:345–351

Gaspar JL, Guest JE, Queiroz G, Pacheco J, Pimentel A, Gomes A, Marques R, Felpeto A, Ferreira T, Wallenstein N (2015) Eruptive frequency and volcanic hazards zonation in São Miguel Island, Azores. In: Gaspar JL, Guest JE, Duncan AM, Barriga FJAS, Chester DK (eds) Volcanic geology of Sao Miguel Island (Azores Archipelago), vol 44. Geological Society, London, pp 155–166 **(Memoirs)**

Gente P, Dyment J, Maia M, Goslin J (2003) Interaction between the Mid-Atlantic Ridge and the Azores hot spot during the last 85 Myr: emplacement and rifting of the hot spot-derived plateaus. Geochem Geophys Geosyst 4:1–23

Giordano D, Russell JK, Dingwell DB (2008) Viscosity of magmatic liquids: A model. Earth Planet Sci Lett 271:123–134

González-García D, Behrens H, Petrelli M, Vetere F, Morgavi D, Zhang C, Perugini D (2017) Water-enhanced interdiffusion of major elements between natural shoshonite and high-K rhyolite melts. Chem Geol 466:86–101

Green NL, Usdansky SI (1986) Ternary–feldspar mixing relations and thermobarometry. Am Miner 71:1100–1108

Guo C, Zhang Y (2016) Multicomponent diffusion in silicate melts: SiO_2-TiO_2-Al_2O_3-MgO-CaO-Na_2O-K_2O system. Geochim Cosmochim Acta 195:126–141

Huber C, Bachmann O, Manga M (2009) Homogenization processes in silicic magma chambers by stirring and mushification (latent heat buffering). Earth Planet Sci Lett 283:38–47

Jeffery AJ, Gertisser R, O'Driscoll B, Pacheco JM, Whitley S, Pimentel A, Self S (2016) Temporal evolution of a post-caldera, mildly peralkaline magmatic system: Furnas volcano, São Miguel, Azores. Contrib Mineral Petrol 171:42

Jeffery AJ, Gertisser R, Self S, Pimentel A, O'Driscoll B, Pacheco JM (2017) Petrogenesis of the peralkaline ignimbrites of Terceira, Azores. J Petrol 58:2365–2402

Johnson CL, Wijbrans JR, Cosntable CG, Gee J, Staudigel H, Tauxe L, Forjaz VH, Salgueiro M (1998) 40Ar/39Ar ages and paleomagnetism of São Miguel Lavas, Azores. Earth Planet Sci Lett 160:637–649

Klügel A, Hoernle KA, Schmincke H-U, White JDL (2000) The chemically zoned 1949 eruption on La Palma (Canary Islands): petrologic evolution and magma supply dynamics of a rift zone eruption. J Geophys Res 105:5997–6016

Klügel A, Hansteen TH, Galipp K (2005) Magma storage and underplating beneath Cumbre Vieja volcano, La Palma (Canary Islands). Earth Planet Sci Lett 236:211–226

Kouchi A, Sunagawa I (1983) Mixing basaltic and dacitic magmas by forced convection. Nature 304:527–528

Kouchi A, Sunagawa I (1985) A model for mixing basaltic and dacitic magmas as deduced from experimental data. Contrib Mineral Petrol 89:17–23

Kueppers U, Pimentel A, Ellis B, Forni F, Neukampf J, Pacheco JMR, Perugini D, Queiroz G (2019) Biased volcanic hazard assessment due to incomplete eruption records on ocean islands: an example of Sete Cidades Volcano, Azores. Submitted to Frontiers in Earth Science **(in review)**

Laumonier M, Scaillet B, Arbaret L, Andújar J, Champallier R (2015) Experimental mixing of hydrous magmas. Chem Geol 418:158–170

Le Maitre RW, Streckeisen A, Zanettin B, Le Bas MJ, Bonin B, Bateman P, Bellieni G, Dudek A, Efremova S, Keller J, Lamere J, Sabine PA, Schmid R, Sorensen H, Woolley R (2002) Igneous rocks: a classification and glossary of terms, 2nd edn, recommendations of the International Union of Geological Sciences, Subcommission of the Systematics of Igneous Rocks. Cambridge University Press, Cambridge, p 236

Luis JF, Miranda JM, Galdeano A, Patriat P, Rossignol JC, Mendes Victor LA (1994) The Azores triple junction evolution since 10 Ma from aeromagnetic survey of the Mid-Atlantic Ridge. Earth Planet Sci Lett 125:439–459

Luis JF, Miranda JM, Galdeano A, Patriat P (1998) Constraints on the structure of the Azores spreading center from gravity data. Mar Geophys Res 20:157–170

Machado F (1959) Submarine pits of the Azores plateau. Bull Volcanol 21:109–116

Manga M (1996) Mixing of heterogeneities in the mantle: effect of viscosity differences. Geophys Res Lett 23:403–406

Mattioli M, Upton BGJ, Renzulli A (1997) Sub-volcanic crystallization at Sete Cidades volcano, São Miguel, Azores, inferred from mafic and ultramafic plutonic nodules. Mineral Petrol 60:1–26

Miranda JM, Luis JF, Fernandes RMS, Lourenço N (2015) The structure of the Azores triple junction: implications for S. Miguel Island. In: Gaspar JL, Guest JE, Duncan AM, Barriga FJAS, Chester DK (eds) Volcanic geology of Sao Miguel Island (Azores Archipelago), vol 44. Geological Society, London, pp 5–13 **(Memoirs)**

Moore RB (1990) Volcanic geology and eruption frequency, Sao Miguel, Azores. Bull Volcanol 52:602–614

Moore RB (1991a) Geologic Map of Sao Miguel, Azores. US Department of the Interior, US Geological Survey, Denver

Moore RB (1991b) Geology of three late quaternary Stratovolcanoes on Sao Miguel, Azores. U.S. Geol Surv Bull 1900:1–46

Morgavi D, Perugini D, De Campos CP, Dingwell DB (2013a) Time evolution of chemical exchanges during mixing of rhyolitic and basaltic melts. Contrib Mineral Petrol 166:615–638

Morgavi D, Perugini D, De Campos CP, Ertl-Ingrisch W, Lavallée Y, Morgan L, Dingwell DB (2013b) Interactions between rhyolitic and basaltic melts unraveled by chaotic mixing experiments. Chem Geol 346:199–212

Morgavi D, Petrelli M, Vetere FP, González-García D, Perugini D (2015) High-temperature apparatus for chaotic mixing of natural silicate melts. Rev Sci Instr 86:1–6

Oliphant TE (2007) Python for scientific computing. Comp Sci Eng 9:10–20

Paredes-Mariño J, Dobson KJ, Ortenzi G, Kueppers U, Morgavi D, Petrelli M, Hess K-U, Laeger K, Porreca M, Pimentel A, Perugini D (2017) Enhancement of eruption explosivity by heterogeneous bubble nucleation triggered by magma mingling. Nat Sci Rep 7:16897

Perugini D, Ventura G, Petrelli M, Poli G (2004) Kinematic significance of morphological structures generated by mixing of

magmas: a case study from Salina Island (Southern Italy). Earth Planet Sci Lett 222:1051–1066

Perugini D, De Campos CP, Dingwell DB, Dorfman A (2013) Relaxation of concentration variance: a new tool to measure chemical element mobility during mixing of magmas. Chem Geol 335:8–23

Perugini D, De Campos CP, Petrelli M, Dingwell DB (2015) Concentration variance decay during magma mixing: a volcanic chronometer. Sci Rep 5:14225. https://doi.org/10.1038/srep14225

Petrelli M, El Omari K, Le Guer Y, Perugini D (2016) Effects of chaotic advection on the timescales of cooling and crystallization of magma bodies at mid crustal levels. Geochem Geophys Geosyst 17:425–441

Petrelli M, El Omari K, Spina L, Le Guer Y, La Spina G, Perugini D (2018) Timescales of water accumulation in magmas and implications for short warning times of explosive eruptions. Nat Comm 9:770. https://doi.org/10.1038/s41467-018-02987-6

Pimentel A, Pacheco J, Self S (2015) The ~ 1000-years BP explosive eruption of Caldeira Volcano (Faial, Azores): the first stage of incremental caldera formation. Bull Volcanol 77:42

Porreca M, Pimentel A, Kueppers U, Izquierdo T, Pacheco J, Queiroz G (2018) Event stratigraphy and emplacement mechanisms of the last major caldera eruption on Sete Cidades Volcano (São Miguel, Azores): the 16 ka Santa Bárbara Formation. Bull Volcanol 80:76. https://doi.org/10.1007/s00445-018-1250-0

Putirka KD (2008) Thermometers and barometers for volcanic systems. In: Putirka KD, Tepley FJ (eds) Minerals, inclusions and volcanic processes. Rev Mineral Geochem Mineral Soc Am 69:61–111

Putirka KD, Perfit M, Ryerson FJ, Jackson MG (2007) Ambient and excess mantle temperatures, olivine thermometry, and active vs. passive upwelling. Chem Geol 241:177–206

Queiroz G (1997) Vulcão das Sete Cidades (S. Miguel, Açores) História Eruptiva e Avaliação do Hazard. PhD Thesis, Azores University

Queiroz G, Pacheco JM, Gaspar JL, Aspinall WP, Guest JE, Ferreira T (2008) The last 5000 years of activity at Sete Cidades volcano (São Miguel Island, Azores): implications for hazard assessment. J Volcanol Geotherm Res 178:562–573

Queiroz G, Gaspar JL, Guest JE, Gomes A, Almeida MH (2015) Eruptive history and evolution of Sete Cidades Volcano, Sao Miguel Island, Azores. In: Gaspar JL, Guest JE, Duncan AM, Barriga FJAS, Chester DK (eds) Volcanic geology of Sao Miguel Island (Azores Archipelago), vol 44. Geological Society, London, pp 87–104 **(Memoirs)**

Raynal F, Gence JN (1997) Energy saving in chaotic laminar mixing. Int J Heat Mass Transf 40:3267–3273

Renzulli A, Santi P (2000) Two-stage fractionation history of the alkali basalt-trachyte series of Sete Cidades volcano (São Miguel Island, Azores). Eur J Mineral 12:469–494

Rhodes JM, Dungan MA, Blanchard DP, Long PE (1979) Magma mixing at mid-ocean ridges: evidence from basalts drilled near 22° N on the Mid-Atlantic Ridge. Tectonophysics 55:35–61

Ridolfi F, Renzulli A, Puerini M (2010) Stability and chemical equilibrium of amphibole in calcalkaline magmas: an overview, new thermobarometric formulations and application to subduction related volcanoes. Contrib Mineral Petrol 160:45–66

Roeder PL, Emslie RF (1970) Olivine-liquid equilibrium. Contrib Mineral Petrol 68:325–334

Rossi S, Petrelli M, Morgavi D, González-García D, Fischer LA, Vetere F, Perugini D (2017) Exponential decay of concentration variance during magma mixing: robustness of a volcanic chronometer and implications for the homogenization of chemical heterogeneities in magmatic systems. Lithos 286–287:396–407

Schilling J-G (1975) Rare-earth variations across 'normal segments' of the Reykjanes Ridge, 60°–53°N, Mid-Atlantic Ridge, 29°S, and East Pacific Rise, 2°-19°S, and evidence on the composition of the underlying low-velocity layer. J Geophys Res 80:1459–1473

Schwarz S, Klügel A, Wohlgemuth UC (2004) Melt extraction pathways and stagnation depths beneath the Madeira and Desertas rift zones (NE Atlantic) inferred from barometric studies. Contrib Mineral Petrol 147:228–240

Sibrant ALR, Hildenbrand A, Marques FO, Weiss B, Boulesteix T, Huebscher C, Lüdmann T, Costa ACG, Catalão J (2015) Morpho-structural evolution of a volcanic island developed inside an oceanic rift: S. Miguel Island (Terceira Rift, Azores). J Volcanol Geotherm Res 301:90–106

Snyder D (2000) Thermal effects of the intrusion of basaltic magma into more silicic magma chamber and implications for eruption triggering. Earth Planet Sci Lett 175:257–273

Snyder DC, Widom E, Pietruszka AJ, Carlson RW, Schmincke HU (2007) Time scales of formation of zoned magma chambers: U-series disequilibria in the Fogo A and 1563 AD trachyte deposits, Sao Miguel, Azores. Chem Geol 239:138–155

Swanson PD, Ottino JM (1990) A comparative computational and experimental study of chaotic mixing of viscous fluids. J Fluid Mech 213:227–249

Wang T, Lin J, Tucholke B, Chen YJ (2011) Crustal thickness anomalies in the North Atlantic Ocean basin from gravity analysis. Geochem Geophys Geosyst 12: Q0AE02

Watson EB (1982) Basalt contamination by continental crust: some experiments and models. Contrib Mineral Petrol 80:73–87

Watson EB, Jurewicz SR (1984) Behavior of alkalies during diffusive interaction of granitic xenoliths with basaltic magma. J Geol 92:121–130

Widom E, Shirey SB (1996) Os isotope systematics in the Azores: implications for mantle plume sources. Earth Planet Sci Lett 142:451–465

Wiesmaier S, Morgavi D, Renggli CJ, Perugini D, De Campos CP, Hess K-U, Ertel-Ingrisch W, Lavallée Y, Dingwell DB (2015) Magma mixing enhanced by bubble segregation. Solid Earth 6:1007–1023. https://doi.org/10.5194/se-6-1007-2015

Zanon V, Frezzotti ML (2013) Magma storage and ascent conditions beneath Pico and Faial islands (Azores Islands): 1. A study on fluid inclusions. Geochem Geophys Geosyst 14:3494–3514

Zanon V, Pimentel A (2015) Spatio-temporal constraints on magma storage and ascent conditions in a transtensional tectonic setting: the case of the Terceira Island (Azores). Am Min 100:795–805

Zhang Y, Ni H, Chen Y (2010) Diffusion data in silicate melts. Rev Mineral Geochem 72:311–408

Affiliations

Kathrin Laeger[1] · Maurizio Petrelli[1] · Daniele Morgavi[1] · Michele Lustrino[2,3] · Adriano Pimentel[4,5] · Joali Paredes-Mariño[1] · Rebecca L. Astbury[1] · Ulrich Kueppers[6] · Massimiliano Porreca[1] · Diego Perugini[1]

1 Department of Physics and Geology, University of Perugia, Piazza dell'Università 1, 06123 Perugia, Italy

2 Dipartimento di Scienze della Terra, Sapienza Università di Roma, P.le Aldo Moro, 5, 00185 Rome, Italy

3 Istituto di Geologia Ambientale e Geoingegneria, CNR, P.le A. Moro, 5, 00185 Rome, Italy

4 Instituto de Investigação em Vulcanologia e Avaliação de Riscos (IVAR), Universidade dos Açores, Rua da Mãe de Deus, Edifício do Complexo Científico, 3° Andar, Ala Sul, 9500-321 Ponta Delgada, Portugal

5 Centro de Informação e Vigilância Sismovulcânica dos Açores (CIVISA), Rua da Mãe de Deus, Edifício do Complexo Científico, 3° Andar, Ala Sul, 9500-321 Ponta Delgada, Portugal

6 Department of Earth and Environmental Sciences, Ludwig-Maximilians-Universität (LMU) Munich, Theresienstrasse 41, 80333 Munich, Germany